POLITECNICO DI TORINO

Collegio di Ingegneria Chimica e dei Materiali

Corso di Laurea Magistrale
in Ingegneria Chimica e dei Processi Sostenibili

Tesi di Laurea Magistrale

Experimental Investigation of Natural Circulation in Multiple Riser and Downcomer Flow Channels in a Simplified High Temperature Gas Reactor Geometry

Relatore

prof. Stefania Specchia
prof. Masahiro Kawaji

Candidato

Giorgio Bologna

Luglio 2023

Contents

Riassunto

La presente Tesi di Laurea Magistrale è il risultato del lavoro svolto dal Candidato durante il periodo Agosto 2022 - Maggio 2023 presso *The City College of New York*, parte della *City University of New York*, sotto la supervisione del Professor Masahiro Kawaji, Professore Emerito del Dipartimento di Ingegneria Meccanica.

L'obiettivo principale del progetto è quello di fornire dati sperimentali riguardo la circolazione naturale di gas tra upper e lower plenum in un *High Temperature Gas Reactor*, ossia un reattore nucleare che utilizza gas come refrigerante e come moderatori di neutroni, simulando una situazione incidentale, a causa della quale il sistema di controllo termico primario non sia in grado di operare, ad esempio per mancanza di elettricità oppure a seguito del malfunzionamento dei dispositivi di circolazione del refrigerante. Si è preso come riferimento il comportamento del 350 MWt MHTGR progettato dalla General Atomics, reattore nucleare di terza generazione con una capacità termica nominale di 350 MW e una capacità elettrica nominale di 165 MW. In questa fase iniziale del progetto, finanziato tra gli altri dal Dipartimento dell'Energia degli Stati Uniti d'America, si è utilizzato azoto gassoso per simulare la circolazione naturale nel sistema, mentre in futuro si prevede l'impiego di elio, il quale viene comunemente usato nei reattori nucleari per svariati utilizzi, tra i quali proprio la refrigerazione. Gli esperimenti sono stati condotti fino a raggiungere 750 °C e 70 bar.

Gli obiettivi principali della seguente Tesi sono quelli di studiare la circolazione naturale del gas tra plenum e plenum in funzione di differenti valori di pressione iniziale e potenza

fornita alle serpentine di riscaldamento, fornendo i valori di velocità del gas utilizzando quattro sensori *thermal time of flight*, uno per ciascun tubo di risalita, e di fornire i profili di temperatura in entrambi i plenum. La velocità che possiede il gas nella sezione di risalita è importante per quantificare la portata massica del gas stesso, a sua volta necessaria per determinare il quantitativo di calore che il gas è in grado di rimuovere dal sistema.

Per quanto di nostra conoscenza, l'apparato sperimentale a nostra disposizione è unico, in termini di complessità e dimensioni; infatti, questo è costituito da 8 tubi paralleli verticali che connettono lower e upper plenum. Quattro di questi, in particolare quelli nella sezione centrale, lunghi all'incirca 2 m l'uno, sono percorsi dal gas che risale e verranno indicati come tubi *risers*, mentre i 4 più esterni, indicati nel seguito come tubi *downcomers*, sono percorsi dal gas che discende. I tubi deputati alla discesa del gas sono leggermente più corti di quelli di risalita, avendo una lunghezza di circa 1.83 m, e sono connessi all'upper plenum usando dei tubi flessibili dalla lunghezza di 0.61 m ciascuno. Questa soluzione è necessaria al fine di tenere conto della differente espansione termica dei tubi, in quanto i risers raggiungono temperature notevolmente superiori a quelle raggiunte dai downcomers.

Ciascun plenum ha un diametro di 0.24 m, mentre l'ingombro totale, che tiene conto anche della piattaforma di supporto, raggiunge circa i 0.47 m. Ogni plenum è alto all'incirca 0.27 m, mentre la camera interna nella quale si dispone il gas ha un'altezza di poco superiore a 0.15 m. Nel seguito viene riportato il disegno tecnico del singolo plenum al fine di facilitare la comprensione della complessa geometria. Un totale di 24 termocoppie viene inserito in ciascun plenum: 16 inserite radialmente nelle due file da 8 termocoppie ciascuna, mentre le rimanenti 8 sono inserite verticalmente, dal basso verso l'alto nel caso del lower plenum per misurare la temperatura all'ingresso dei tubi, oppure dall'alto verso il basso nel caso dell'upper plenum, per misurare la temperatura del gas all'uscita di ciascun tubo.

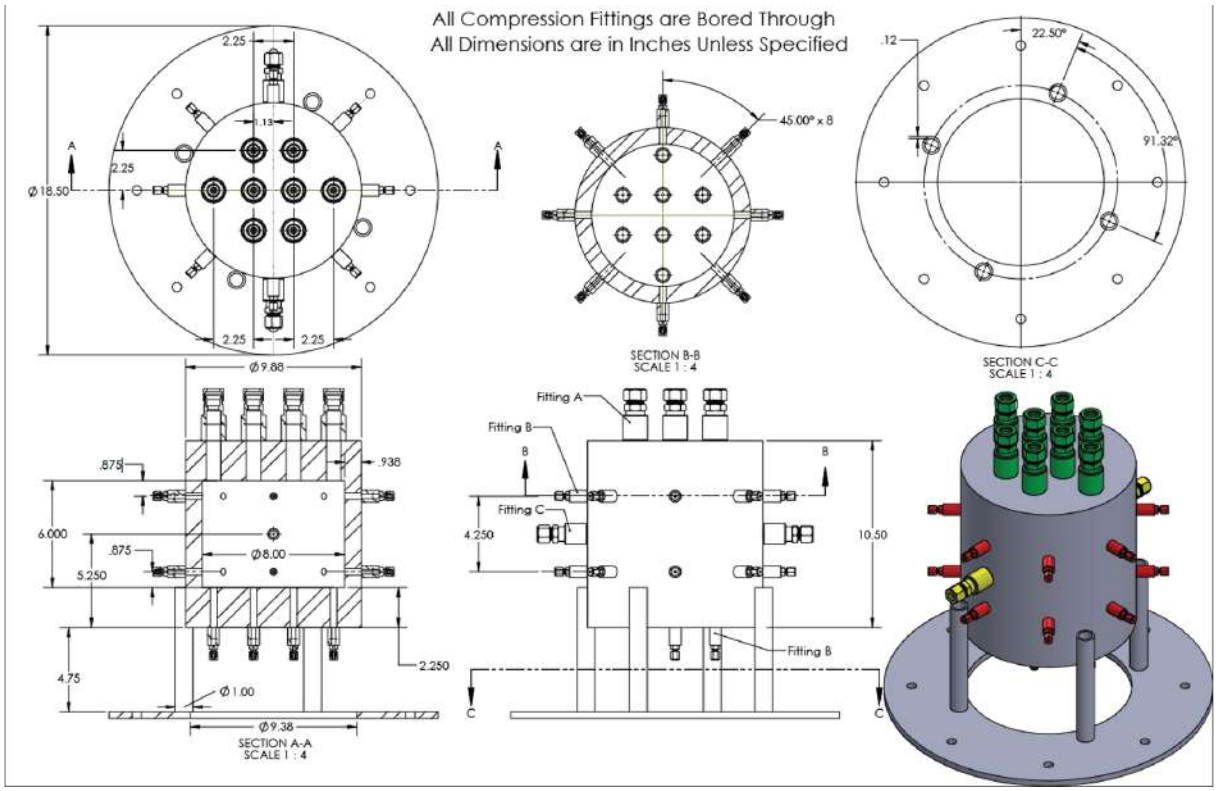

Figure i: Plenum schematic

Ogni tubo è dotato di una serpentina di riscaldamento della lunghezza di 7 m; quelle montate sui tubi riser sono indipendenti le une dalle altre, essendo collegate ognuna ad un variac diverso, mentre quelle montate sui tubi downcomer sono alimentate a coppie da solamente due variac diversi. Questa scelta è giustificata dal fatto che, per massimizzare la circolazione naturale del gas all'interno del sistema, si vuole avere la massima differenza di temperatura tra tubi riser e tubi downcomer, tanto che nella maggior parte degli esperimenti condotti i downcomers non sono neanche stati riscaldati. Infine, due termocoppie sono state saldate su ciascun tubo, al fine di monitorare la temperatura superficiale degli stessi, a due altezze differenti.

Un aspetto fondamentale per la riuscita dell'esperimento è l'isolamento termico del sistema. Per questo motivo, si è scelto di utilizzare un isolamento termico in fibra di vetro, che rappresenta il miglior compromesso in termini economici e di prestazioni. In questa fase iniziale dell'esperimento entrambi i plenum e i tubi di risalita sono stati avvolti dalla fibra di vetro, mentre i tubi downcomer sono rimasti esposti all'ambiente circostante,

sempre al fine di massimizzare la circolazione naturale del gas. Non è da escludersi che in futuro possano essere avvolti dall'isolamento termico anche i downcomers. Si faccia riferimento alle Figure del Capitolo 2 per chiarire eventuali dubbi relativi al setup presente al *City College of New York* e precedentemente descritto.

Come brevemente citato in precedenza, uno degli obiettivi del progetto è quello di sviluppare dei misuratori di velocità che siano indipendenti dalla tipologia di gas utilizzato e dalle condizioni di temperatura e pressione. A tal fine, si sono sviluppati 4 sensori, ciascuno installato su un tubo riser, che basano il loro principio di funzionamento sul cosiddetto "tempo di volo". Viene introdotto un impulso termico nel fluido in movimento e si determina la velocità dello stesso calcolando il tempo necessario affinchè due o più termocoppie poste downstream a distanza nota rilevino l'incremento istantaneo di temperatura. L'apparato sperimentale per ciascun sensore utilizzato è composto da tre termocoppie saldate nel tubo, un filo di NiChrome attorciliato a formare un'elica collegato ad un generatore di corrente alternata e ad un dispositivo in grado di generare periodicamente nel tempo l'impulso elettrico.

Trovare analiticamente una soluzione al problema del trasporto dell'impulso termico per il calcolo della velocità del gas è molto complesso, in quanto richiede la risoluzione di un sistema di equazioni differenziali alle derivate parziali per le quali risulta indispensabile inizializzare alcuni parametri dipendenti dalla velocità stessa. Per questo motivo, la velocità del gas è stata calcolata utilizzando la cross-correlation tra le serie di dati registrate dalle singole termocoppie. Infatti, questo metodo ha permesso di identificare serie di dati tra loro correlate e di quantificare di quanto fossero sfasate temporalmente tra loro.

Essendo ciascun sensore time of flight fabbricato in laboratorio senza strumenti di precisione, un processo di calibrazione è stato necessario prima dell'installazione degli stessi nel setup della circolazione naturale. I risultati vengono riportati nelle Figure 3.6-3.9. I grafici confermano proprio il comportamento peculiare di ciascun sensore per via della ragione sopra esposta. Infatti, essendo il flusso in regime laminare, è ragionevole aspettarsi un profilo parabolico della velocità, e di conseguenza la posizione radiale dell'elemento sensibile

di ogni termocoppia gioca un ruolo fondamentale nella determinazione della velocità.

Il quarto Capitolo è invece incentrato sulla circolazione naturale e sui risultati sperimentali ottenuti in laboratorio. Per circolazione naturale si intende la movimentazione di un fluido, generalmente un gas o un vapore, soggetto a gradienti di densità indotti a loro volta dall'esposizione del fluido stesso a differenti temperature in diverse regioni del sistema. Un loop di circolazione naturale è schematicamente costituito da una fonte di calore, uno scambiatore di calore e una serie di due o più tubi che colleghino gli ambienti precedentemente citati. In pratica, nei reattori nucleari la fonte di calore è rappresentata dal *reactor core*, mentre il generatore di vapore riceve il calore prodotto dalla reazione nucleare consentendo di mantenere la temperatura dell'intero reattore nei limiti operativi.

La circolazione naturale è considerata uno dei più importanti sistemi di sicurezza passivo disponibili. Ciò significa che consente di rimuovere calore dal nucleo del reattore nucleare sia durante le operazioni di shutdown che in quelle di emergenza, senza l'impiego di apparecchiature esterne per la movimentazione dei fluidi, come ad esempio pompe e compressori, che ragionevolmente non sono disponibili durante una situazione incidentale. Ci sono numerosi vantaggi e alcune limitazioni nell'utilizzo della circolazione naturale come *passive safety system*; anche se un'analisi dettagliata è riportata nel Capitolo 4, gli aspetti più importanti verranno discussi nel seguito. Innanzitutto, la circolazione naturale non necessita di apparecchiature per la movimentazione dei fluidi, riducendo i costi d'investimento, delle operazioni e di manutenzione. In secondo luogo, è sempre disponibile essendo un fenomeno fisico basato su gradienti di densità. In aggiunta, a differenza della circolazione forzata, quella naturale ha teoricamente una migliore distribuzione del flusso in canali verticali, comunemente utilizzati nei reattori nucleari. Di contro, la più grande limitazione della circolazione naturale è la sua intrinseca limitata forza spingente, fattore che spinge gli esperti del settore ad investire tempo e risorse nella ricerca e sviluppo al fine di garantire che questo sistema di sicurezza passivo sia sufficiente a rimuovere il calore prodotto dal nucleo del reattore in maniera efficace e sicura. In aggiunta, la circolazione naturale soffre di un'intrinseca instabilità del flusso, ossia oscillazioni nella portata di gas

sono attese nel tempo.

Alcuni esperimenti preliminari sono stati condotti prima di testare il loop di circolazione naturale, in particolare il test di tenuta a pressione e il test delle perdite di calore.

Il primo viene condotto pressurizzando il sistema fino a raggiungere il limite nominale, vicino ai 70 bar (o equivalentemente 1000 psi) e registrando l'andamento della pressione con il tempo. È ragionevole pensare che la pressione diminuisca per la presenza di perdite nelle giunzioni, e ci si aspetta che quelle di elio siano maggiori di quelle di azoto, per via delle proprietà chimico-fisiche dei due gas usati. Questo andamento viene confermato dai grafici riportati nelle Figure 4.1 e 4.2. In particolare, per l'elio le perdite ammontano a 4.14 bar h^{-1}, mentre per l'azoto a 9.10×10^{-1} bar h^{-1}. Entrambi i risultati sono soddisfacenti ai fini degli esperimenti sulla circolazione naturale che verranno discussi nel seguito.

Per quanto riguarda il test delle perdite di calore, tutti i tubi vengono riscaldati e si porta la temperatura di ciascun tubo a raggiungere un valore stazionario nel tempo, condizione nella quale il calore fornito dalle serpentine di riscaldamento eguaglia quello dissipato verso l'ambiente esterno. Per questo test è necessario portare il sistema in condizioni di vuoto, in quanto la presenza di gas all'interno modificherebbe l'equilibrio tra calore fornito e calore dissipato per via della capacità intrinseca del fluido stesso di rimuovere calore. I risultati dei test sono riportati nelle Figure 4.3-4.6, dove si presenta l'andamento del calore dissipato come funzione della temperatura di stato stazionario. Si può notare che i tubi riser 1 e 2 hanno sostanzialmente lo stesso comportamento, mentre i tubi riser 3 e 4, con andamento simile tra loro, hanno delle perdite di calore notevolmente maggiori rispetto a quelle dei primi due. La ragione principale che giustifica questa disparità sta nel fatto che l'isolamento termico è stato manualmente montato nella struttura e sicuramente alcune zone sono risultate meglio coperte di altre. Per quanto si sia provato a migliorare la performance di isolamento termico per i tubi riser 3 e 4, i risultati non hanno mai mostrato un miglioramento sostanziale e per questo motivo si è deciso di andare avanti con gli esperimenti tenendo semplicemente conto del diverso comportamento tra i tubi riser.

In questa fase iniziale del progetto, solamente l'azoto è stato usato per gli esperimenti di circolazione naturale, per via della disponibilità maggiore dello stesso rispetto all'elio e per il prezzo minore rispetto al secondo. La Tabella 4.1 riporta le condizioni sperimentali investigate durante questa Tesi.

Gli obiettivi di questa sezione sono due: il primo è quello di definire i profili di temperatura e pressione all'interno del sistema per differenti condizioni operative, e verificare che non vi siano anomalie nella distribuzione del gas. Il secondo è invece quello di testare i sensori time of flight per la misurazione della velocità del gas, confrontando le loro misurazioni con i valori attesi di velocità calcolati a partire da un bilancio di energia. Quest'ultimo si basa sulla seguente relazione:

$$\dot{Q}_{supplied} = \dot{Q}_{loss} + \dot{Q}_{gas} \tag{1}$$

dove $\dot{Q}_{\text{supplied}}$ rappresenta il calore fornito dalle serpentine di riscaldamento, $\dot{Q}_{\text{loss}}$ il calore disperso nell'ambiente circostante, calcolato con le curve di regressione che interpolano i dati sperimentali del *heat loss test* e $\dot{Q}_{\text{gas}}$ quello rimosso dal gas che si muove per circolazione naturale. I profili di temperatura e pressione sono mostrati nelle Figure 4.8-4.22. Alcune di queste presentano un andamento tipico, comune a tutti gli esperimenti, ottenuto per una specifica condizione sperimentale, mentre altre mostrano come le variabili di maggiore interesse varino in funzione delle condizioni operative e del valore iniziale di pressione dell'azoto gassoso.

L'obiettivo di ciascun esperimento è quello di raggiungere una condizione di stato stazionario, anche se ciò non sempre è possibile, specialmente per i profili di temperatura nel lower plenum. In questa sezione, infatti, il raggiungimento dello stazionario richiederebbe di performare gli esperimenti per più di 12 ore consecutive, non compatibili con la lunghezza della giornata lavorativa e con le performance del sistema di raccolta dati che verrebbe inevitabilmente sovraccaricato con il rischio di perdere tutti i dati precedentemente raccolti. Tuttavia, i profili sono ben definiti ed è ragionevole aspettarsi che questi non varino significativamente dalla condizione di semi-stazionarietà a quella di completa stazionarietà.

I risultati più interessanti verranno brevemente presentati qui di seguito.

Nel lower plenum, il gas è radialmente ben miscelato, il che significa che per una determinata sezione ad un'altezza scelta la temperatura risulta essere uniforme. È invece presente un gradiente verticale, poichè il gas meno caldo tende a stratificare sul fondo del plenum, mentre quello più caldo a disporsi in prossimità dei tubi riser. Un andamento molto simile viene riscontrato anche nell'upper plenum, confermando quindi come non vi sia una perfetta miscelazione per le condizioni sperimentali investigate. I profili di temperatura della superficie esterna dei tubi invece confermano quanto trovato con i test delle perdite di calore, tenendo comunque in considerazione che i tubi riser ricevono ciascuno una potenza termica che è leggermente differente da quella degli altri. Infine, i profili di temperatura più interessanti sono quelli del gas all'ingresso e all'uscita dei tubi (Figure 4.19-4.24). Il risultato più eclatante in questo caso è che i dati sperimentali confermano la presenza della circolazione naturale, avendo picchi di temperatura all'uscita dei tubi riser, dove il gas risale riscaldandosi, e valori maggiori di temperatura all'ingresso dei tubi downcomer, nel lower plenum, significando quindi che il gas caldo scende negli appositi tubi, installando appunto la circolazione naturale tra lower e upper plenum.

Infine, vengono riportati i risultati relativi ai sensori di velocità. In particolare, le Figure 4.27-4.32 mostrano un confronto tra la velocità calcolata dal bilancio di energia e quella calcolata dal sensore al variare delle condizioni sperimentali, per i tubi riser 1, 3 e 4. I dati per il sensore time of flight sul tubo riser 2 sono mancanti in quanto è stato installato al suo posto un altro sensore, basato su principi ottici, sviluppato dall'Università di Pittsburgh, partner del progetto. Purtroppo, il loro *optical fiber sensor* ha subito un danneggiamento nelle prime fasi di utilizzo e non è quindi stato possibile confrontare i valori calcolati dai diversi sensori. I risultati più interessanti per i sensori di velocità sono riportati brevemente nel seguito. In primo luogo, la velocità calcolata con il bilancio di energia risulta essere sempre significativamente maggiore di quella calcolata dai sensori time of flight, indipendentemente dalle condizioni sperimentali. Tuttavia, l'andamento della velocità al variare della potenza immessa nelle serpentine di riscaldamento è comune

tra le due misurazioni e l'errore relativo, specialmente per i sensori montati sui tubi riser 1 e 3, è di poco inferiore al 30%. Infine, la velocità all'interno del loop dipende dalla pressione operativa: al diminuire della pressione iniziale del gas aumenta la velocità calcolata, poichè le molecole del gas sono meno compatte e offrono una minor resistenza al movimento del gas stesso.

In futuro, ulteriori esperimenti sulla circolazione naturale verranno condotti nel setup al City College di New York, testando differenti condizioni di pressione iniziale e potenza fornita alle serpentine di riscaldamento. Inoltre, vi è l'intenzione di utilizzare elio e una miscela di elio e azoto per simulare più accuratamente il comportamento di un reattore nucleare reale. Inoltre, il team di ricerca dell'Università di Pittsburgh (*Pittsburgh University*) installeranno un secondo sensore di velocità da loro sviluppato, in modo tale da avere due sensori *time of flight* e due sensori *optical fiber* e poter confrontare l'accuratezza dei due metodi di misura. Infine, il team di ricerca dell'Università Statale dell'Idaho (*Idaho State University*) fornirà un'analisi dettagliata sullo scale-up del sistema, in modo tale da verificare l'efficacia della circolazione naturale nella rimozione di calore non solo su scala di laboratorio ma anche per un reattore nucleare reale.

Chapter 1

Introduction

The main objective of this experimental investigation is to obtain and provide experimental data on the plenum-to-plenum natural circulation (NC) flows in a High Temperature Gas Reactor (HTGR), such as a General Atomics 350 MWt MHTGR. Early in 2001, the United States Department of Energy (U.S.DOE) defined the Very High-Temperature Reactor (VHTR) "as a system with potential for economical near-term development that is compatible with advanced electricity and hydrogen production, and high-temperature process-heat applications".

Nowadays, mainly due to the Russian invasion on Ukraine territories began at the end of February 2022, the energy sector is facing critical issues, especially in European countries. In fact, in 2020 more than 58% of Europe's available energy was produced in non-EU member states.

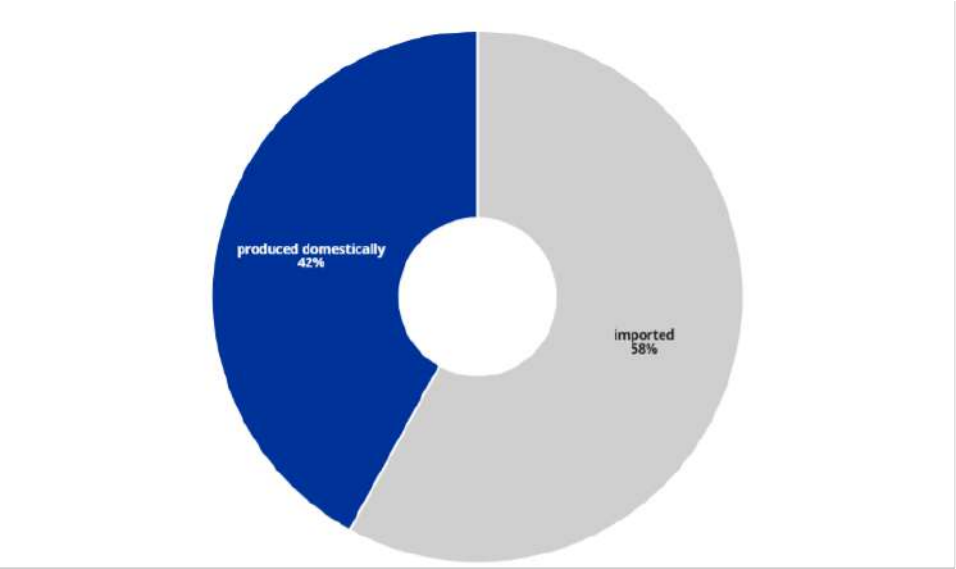

Figure 1.1: Energy distribution in Europe

According to data from the European Union, about 40% of the energy produced nationwide came from renewable sources, as about 30% from nuclear plants. The country from which most of the energy is imported from is Russia, as 43% of gas and 54% of coal come from the Russian Federation. After several months of conflict and as a result of sanctions imposed by U.S. Department of State and most European governments, the Russian Federation is about to stop the furniture of both gas and coal, leading the European continent into a period of uncertainty from the energetic point of view. As the energy crunch hits Europe, the issue of energy independence becomes increasingly important, lest any such escalation in the future lead to similar situations, and for this reason governments of the so-called 'Old Continent' are analyzing all possible solutions so that the situation does not degenerate to the point of power failure. Among them, re-activation of already present nuclear plants and construction of new ones are considered.

All the cited information is shown in the following graph.

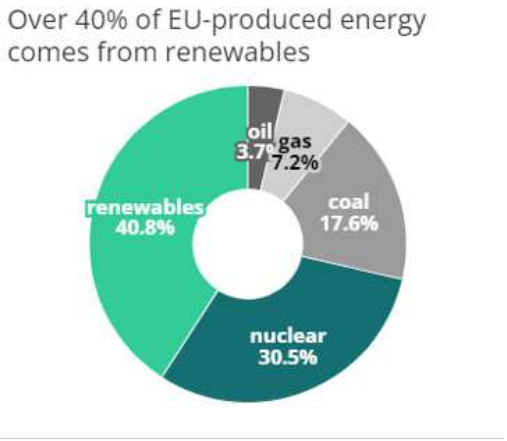

Figure 1.2: Breakdown of energy produced domestically in the European Union

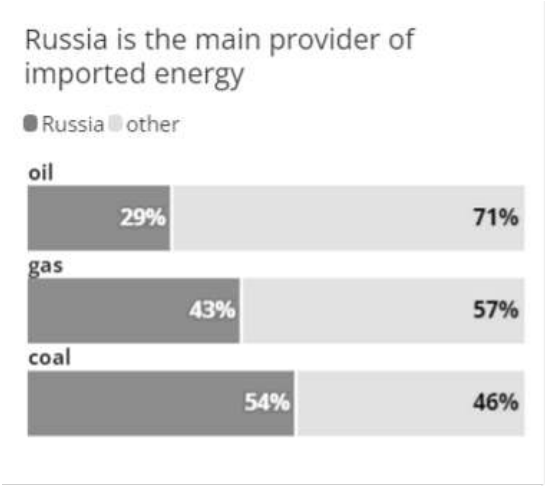

Figure 1.3: Percentage of imports from Russia and other countries

Historically, Europeans perception of nuclear plants is controversial, depending on the country considered, mainly because of the terrible and devastating consequences resulting from the Chernobyl disaster occurred on 26 April 1986 at the Chernobyl Nuclear Plant Power in the Ukrainian SSR in the Soviet Union. A study carried out by 'Agenzia Nazionale per le Nuove Tecnologie, l'Energia e lo Sviluppo Economico Sostenibile', supervised by the Italian Ministry of Ecological Transition (Ministero della Transizione Ecologica) pointed out that the greater the knowledge of the issues, the greater the popular consensus. In fact, in countries where information about nuclear power is constant and aimed at all citizens there is a greater approval - well above 50% - and this is the case of Sweden, France, Finland and Belgium; in the contrary, a clear opposition is registered in countries where there is little discussion about this topic.

The chemical element Uranium is the fuel used in a nuclear power reactor, as it stores high amount of energy per unit mass and, among the three isotopes, one of them, uranium-235, is fissile, that is it can split during the fission process, which realizes considerably more energy than any other combustion process. In particular, the nucleus of an atom of U^{235} splits into two smaller nuclei when hit by a neutron, with the formation of spares neutrons, which have the ability to move and make contact with other uranium-235 nuclei, in a multiplying effect resulting in a chain reaction.

In nuclear power plants, ceramic pellets of uranium fuel are used in the reactor core stacked together into sealed metal tubes, the latter immerged in water which is heated up by the heat released in the reaction to produce steam, which in turn spins a turbine producing very small carbon-footprint energy.

Since 2001, Research and Development (R&D) efforts on Nuclear Power Plants (NPPs) have been joined together in an international collective, called Generation IV International Forum (GIF), representing different governments in the world, which commitment is to share valuable information and funds for developing newer safe, sustainable and cost-effective nuclear reactor designs.

Late in 2002, six different nuclear reactor designs have been proposed as the future for nuclear energy, having the above-cited characteristics. These reactor designs differ from each other in terms of coolant, efficiencies, operating conditions and electrical power productions but most of them use a fuel closed loop, in order to maximize the energy source and minimize highly toxic wastes disposal.

The main characteristics of these six new designs will be listed below, focusing then on Very High Temperature Reactors (VHTRs).

- Sodium Fast Reactors
- Super-critical water-cooled Reactors
- Gas-cooled Fast Reactors
- Lead-cooled Fast Reactors
- Molten Salt Reactors
- Very High Temperature Reactors

1.1 Sodium Fast Reactors

Sodium Fast Reactors (SFRs) are fast reactors cooled using liquid sodium. Fast reactor are

nuclear reactors in which neutrons are maintained at very high kinetic energy levels and for this reason they do not require a neutron moderator to be present in the system. The main advantage related to this technology is that it is possible to increase the efficiency of usage of nuclear fuel by converting fertile material in fissile. Moreover, it has been underlined that fast reactor's wastes decay much faster than traditional reactor's ones. Additionally, using a metal liquid coolant, with very high heat-transfer properties, instead of water allows natural circulation to remove heat in the case of loss of forced convection, that happens when the cooling system shuts down for major reasons.

In contrary, the usage of coolants such as liquid sodium or liquid lead-bismuth eutectic, derived from heavy atoms and generally highly reactive with water and air at operating conditions, implies that particular attention must be given to the system's safety. In addition, fast reactors may go through unpredicted changes in operating conditions faster than other nuclear reactor designs, because there are fewer delayed neutrons in this configuration.

1.2 Super-critical Water-cooled Reactors

Super-critical Water-cooled Reactors (SCWRs) are thermal or fast reactors using supercritical water as coolant. This solution is being studied because water, above 374 °C and 22.1 MPa, has excellent heat transfer properties and allows the usage of a *supercritical Rankine cycle*, which has improved efficiencies. Compared to the previous concept of Generation III Boiling Water Reactors (BWRs), a Super-critical Water-cooled Reactor has higher net electrical efficiency (up to 10% higher, 44% or more, compared to 34-36% for current reactors). Also, the usage of supercritical water allows the reduction of required components such as steam dryers and recirculation system, because supercritical water can be directly used in steam turbine and the phase transition of boiling is not required. The biggest concern related to this configuration lies in the fact that the use of supercritical water brings corrosion problems into the system and for this reason higher costs for maintenance are expected. Moreover, the combination of high temperatures and pressures puts the components under higher mechanical and thermal stresses, thus raising

prices at the design stage.

Different configurations of super-critical water-cooled reactors are being investigated in projects that are being developed in recent years. The description of the different technical characteristics is beyond the scope of this discussion and therefore they will not be discussed in detail.

1.3 Gas-cooled Fast Reactors

Gas-cooled Fast Reactors (GFRs) are high-temperature helium-cooled fast-spectrum reactors with fuel closed cycle. This solution is practically a combination of fast-spectrum and high-temperature systems. Consequently, it has the advantages of both latter, such as long-term sustainability of uranium resources, waste minimization, high thermal cycle efficiency and industrial usage of generated heat.

Generally, the coolant used in a gas-cooled fast reactor is helium, and temperatures in the order of 800-900 °C are expected at the reactor core outlet. This thermal energy is transferred to a mixture of helium and nitrogen in gas phase, to run a closed cycle gas turbine. As it happens frequently in high temperature systems, the waste heat at the outlet of the gas turbine is used to heat up steam in a steam generator to drive a steam turbine. It is common to adopt a Brayton cycle, with few different compression steps, from the low-pressure compressor to the high-pressure compressor. At the outlet of each single compression state, helium gas undergoes a process of cooling in a compressor intercooler, because the higher density of cool gas makes it easier to compress than a hot one. After passing through the hot side of a heat exchanger, helium faces few steps of expansion in successive gas turbines, to produce electricity.

1.4 Lead-cooled Fast Reactors

Lead-cooled Fast Reactors (LFRs) are fast reactors cooled using lead or lead-bismuth eutectic. Both latter have high boiling point, making them appropriate coolant in nuclear power plant applications. Moreover, experimental trials have demonstrated that the use

of lead facilitates natural convection phenomena, simplifying heat transfer processes and enhancing intrinsic safety.

The biggest concern about this configuration is related to coolant's safety issues. In fact, lead is a toxic material and its waste disposal need to be treated carefully. Moreover, both coolants are highly corrosive. About the different characteristics, pure lead is less expensive, more abundant and less corrosive, but has a melting temperature significantly higher than lead-bismuth eutectic's one, and for this reason the latter is taken in consideration, to avoid the solidification of the coolant in the reactor core during transition phases. However, it has to be underlined that there is an evolution from the LBE technology towards the pure lead one, because of both economical and safety improvements.

European Union ELSY (European Lead-cooled System) led to a first proposal of lead-cooled fast reactor, producing a thermal power of 1500MW by using uranium and plutonium and burning their own generated minor actinides (MAs) as well.

1.5 Molten Salt Reactors

Molten Salt Reactors (MSRs) are nuclear reactors cooled using molten salts and they can be either fast or thermal reactors. The main characteristic of this technology is that the nuclear fuel is in liquid phase, dissolved in the molten fluoride salt coolant. Even though this technology is well-known since the 1950s, modern interest is focused on them as long term alternative to fast neutron reactors using solid fuel. This leads to significant advantages from operational, safety and economic point of view; the following are the most important: 1) possibility to online refuel the reactor, 2) does not require the fabrication process for the fissile material, thus reducing the costs and criticalities, 3) a lower mass of fissile material improves safety conditions in the plant, because the fuel can be taken out from the reactor at any time.

On the contrary, having the coolant in direct contact with the fissile material brings the attention to coolant treatments. In fact, reaction by-products, such as lanthanides, noble gases and noble metals, must be removed from the cooling fluid. In order to remove noble

gases and noble metals, helium gas is injected into the system, while for separating the lanthanides and actinides a off-line facility is needed lifting up the price of equipment and operations. In addition, molten salts are corrosive, and this characteristic is even more accentuated by the contact with oxidized fission products.

Different projects on Salt Molten Reactors are at Research & Development stage on both nuclear and non-nuclear applications. Among them, nuclear hydrogen production concepts, concentrated solar electricity generation, oil refineries and shale oil processing facilities.

1.6 Very High Temperature Reactors

Very High Temperature Reactors (VHTRs) are nuclear systems working with temperatures up to 1000 °C. High temperature reactors are interesting since they reach high net electrical efficiency, meaning that the ratio between the electrical power delivered to the grid and the thermal produced one is high. Moreover, they are orientated to co-generation and hydrogen production. A VHTR is a graphite-moderated, helium-cooled reactor with thermal neutron spectrum. Helium is used because of high thermal conductivity and specific heat and finally because it is radiologically and chemically inert, stable in project's operating conditions. Thermally speaking, graphite and helium have the same properties, so the first one is used as moderator because it helps slowing down transitions in accidental situations.

Among the six different GEN IV technologies already listed, Very High Temperature Reactors are the only ones suitable for hydrogen production, generally using steam electrolysis, but studies are still at early stages, and R&D is needed for heat exchangers, coolant gas ducts and valves, as well as safety issues. Moreover, current market assessments have pointed out that electricity production, along with steam production for industrial processes, seem to be the most promising pathways for this technology, requiring modest outlet temperatures (700-850 °C) and implying reduced technical issues associated with very high temperatures.

Two different main configurations have been studied in recent years, and these are the *pebble bed* (PB) and the *prismatic block core*. Briefly, a prismatic block core has a better neutronic stability and produces less dust than a pebble bed, while the latter has lower operating temperatures, allowing the use of conventional steel, and it has a higher capacity factor, meaning that it operates at maximum capacity for a longer time than the prismatic block core. Surely, these considerations are from a simplified perspective, and the choice of either configuration will be based on much deeper considerations and understandings.

Last but not least, Generation IV International Forum (GIF, 2012) proposes other applications, such as coal liquefaction and desalination, which viability has not been defined yet.

As stated by the Gen IV International Forum, "the VHTR is the next step in the evolutionary development of high temperature gas-cooled reactors". One example of VHTRs is the General Atomics' Prismatic Modular HTGR module, which has been taken as reference for this project. This gas-cooled reactor uses helium as coolant and graphite as moderator, delivering a thermal capacity of 350MW(t) and a Gross Electrical Capacity of 150MW(e).

The active core of the reactor has a hexagonal shape with graphite fuel elements, with 210 holes for fuel compacts and 102 channels for the coolant to flow through.

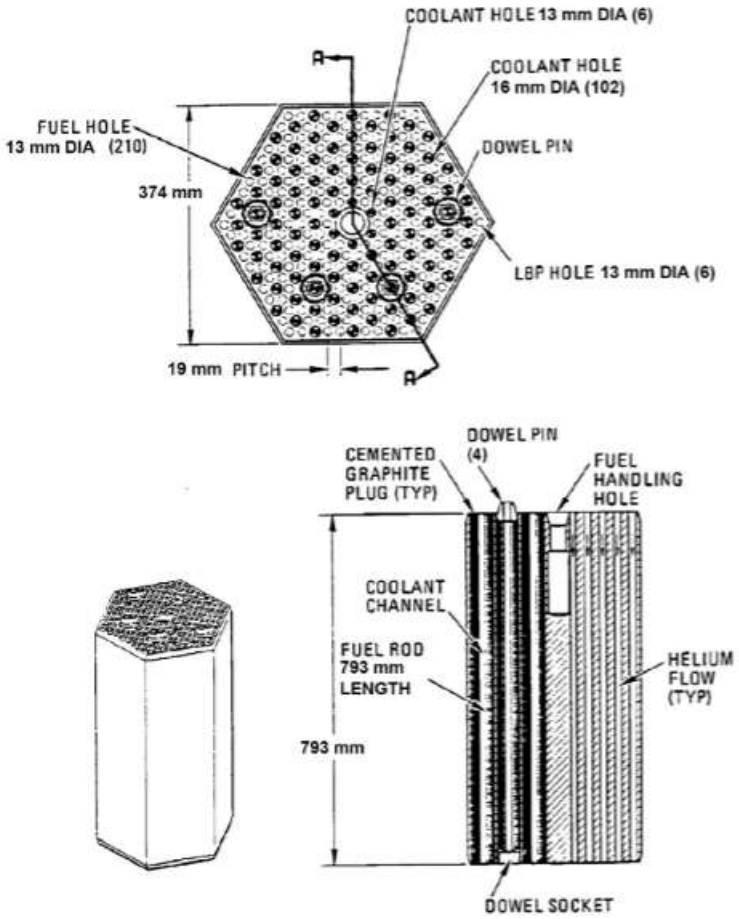

Figure 1.4: Reactor Core Subsystem

In this system, TRISO (Tri-structural ISOtropic) coated fuel particles are used in cylindrical compacts, held together with a carbonaceous matrix to form fuel pellets, and stacked together to form columns. Coating on fuel particles has an important function, as it can retain fission products at very high temperatures without degradation. In fact, coating do not start to degrade until temperatures of about 2000 °C are reached.

The General Atomics' Prismatic Modular HTGR Module uses Uranium oxycarbide (UCO) enriched in uranium as fuel to deliver a Module Power of 350MW(t). Around $157\,\mathrm{kg\,s^{-1}}$ of helium coolant flow through the reactor core and it is reasonable to predict that gas helium coolant has a variation in temperature of about 400 °C between inlet and outlet, reaching 750 °C at core outlet.

In this configuration, the Heat Transport System (HTS) unit consists of the Steam-

Generator Subsystem and the Main Circulator Subsystem. The first one is a heat exchanger with a nominal heat duty capacity of 352MW(t) and it is located below the reactor core. Instead, the circulator is an electric motor driven compressor unit and it is submerged in the helium coolant.

During the time when the Heat Transfer System is non-operational, the Shutdown Cooling System cools down the reactor. It primarily consists of a shutdown circulator, a shutdown cooling control and a water-cooled shutdown heat exchanger, which uses water to cool down helium gas and heat is rejected to the plant service water system.

Lastly, a passive safety-related system has been implemented and it is called *Reactor Cavity Cooling System* (RCCS). It has been designed in such a way as to remove heat during accident scenarios, when either the Heat Transport System or the Shutdown Cooling System can not work. For this reason, it consists of cooling panels, inlet and outlet structures and a concentric duct system in order to establish a natural convection airflow, thanks to a balance of buoyancy and gravitational forces, without needing any active component, such as pumps, circulators or valves. Decay heat is removed by conduction to the pressure vessel and transferred by radiation from this vessel to the reactor cavity cooling system, which operates only with natural circulation [9].

Passive Safety Systems

Historically, electric or Diesel motors have been used during accident scenarios, especially in the case of *reactor scram*, i.e. the rapid insertion of control rods into the reactor core to immediately stop the fission reactor and shut the reactor down.

However, over the last decades, passive safety systems have gained more importance, because they can be activated during accidental scenarios without any external input.

According to IAEA-TECDOC-1624, 'a passive system is defined as either a system, which is composed entirely of passive components and structures, or a system, which uses active components in a very limited way to initiate subsequent passive operation'. The Inter-

national Atomic Energy Agency (IAEA) has identified four categories of passive safety systems; they are the following:

- Category A passive safety features 'are those, which do not require external signal inputs of "intelligence", or external power sources or forces and have neither any moving mechanical parts nor any moving working fluid'.

- Category B passive safety features 'are those which do not require external signal inputs of "intelligence", or external power sources or forces, and have no moving mechanical parts. They do, however, have moving working fluids'.

- Category C passive safety features 'are those which do not require external signal inputs of "intelligence", or external power sources or forces. They do, however, have moving mechanical parts whether or not moving working fluids are present'.

- Category D passive safety features, referred to as "passive execution/active initiation" 'are those passive features where the execution of the safety function is made through passive methods as described in the previous categories except that internal intelligence is not available to initiate the process'.

Among them, particular attention has been given to natural circulation phenomena. Natural circulation is a heat transfer process in which residual heat from the reactor core can be removed by fluids moving only by effect of gravitational and buoyancy forces. Newly projects on nuclear power plants tend to include natural circulation systems as one of the principal passive safety features [6].

Natural circulation has been given increasing attention because of the simplicity of the system itself, since it does not involve any active power supply, in particular pumps. This characteristic is fundamental, because it lowers operational and maintenance costs, and moreover pumps would not work during accidental scenarios. In addition, accidents may cause piping and machines to get damaged. Lastly, considering the inlet pressure to be constant, the fluid distribution within the core tubes is uniform [6].

Chapter 2

Test and Instrumentation Section

A deep insight into the design of the reference General Atomics' 350 MWt MHTGR is not the purpose of this thesis, but a brief description of some of the technical and geometrical characteristics is needed to better understand the following discussion.

The reactor is designed for an Installed thermal capacity of 350 MW(t) and an Installed electric capacity of 165 MW(e). The reactor vessel has a height of 22 m and an outside diameter of 6.8 m. As already mentioned in the introduction chapter, the primary coolant is Helium, fed into the system at a nominal pressure of 6.39 MPa. Moreover, 687 °C and 259 °C are the core outlet temperature and core inlet temperature, respectively.

Our facility setup aims to model the flow characteristics of the refrigerant inside the reactor core. Specifically, major interest is directed toward modeling the plenum to plenum natural circulation flows under both Pressurized and Depressurized Conduction Cooldown events in a scaled down system.

In the following, a schematic of the system is shown.

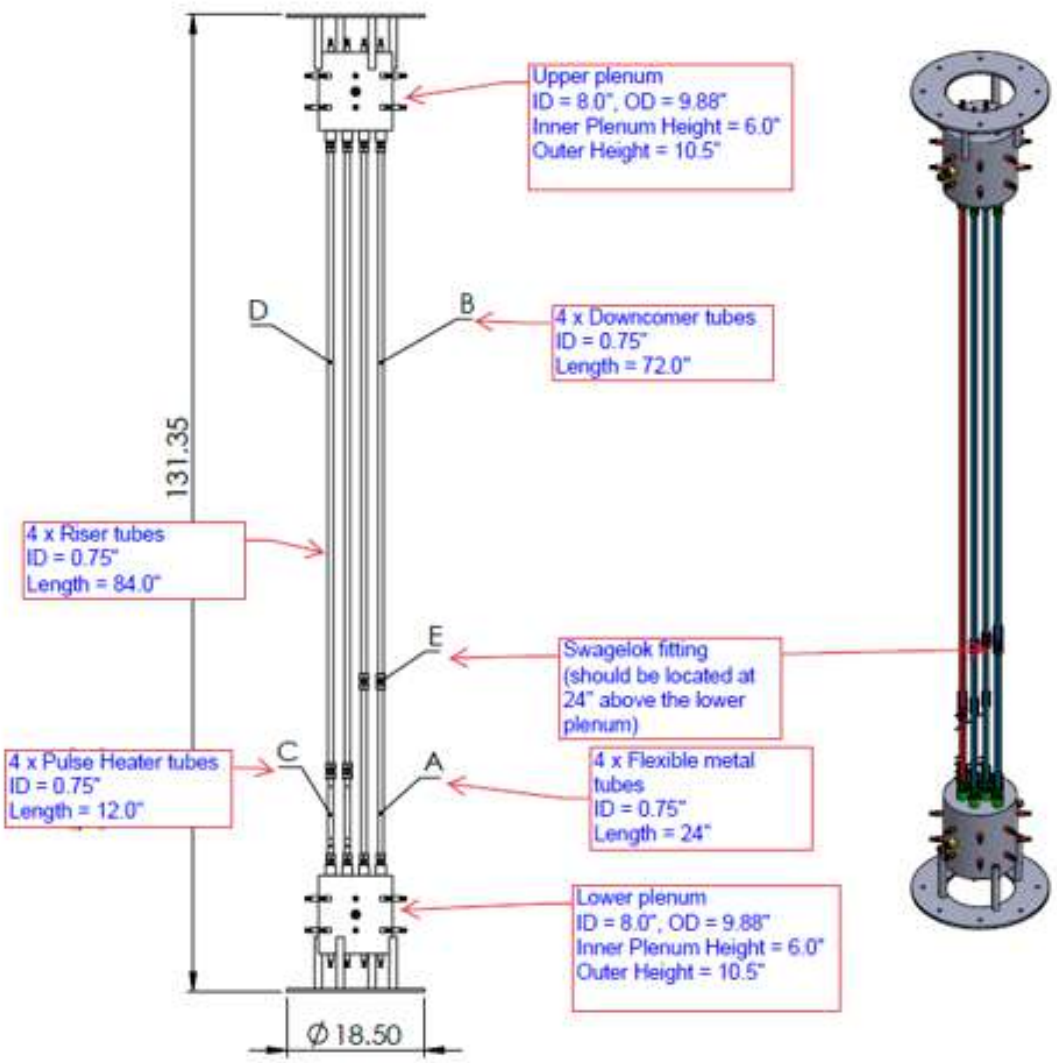

Figure 2.1: System schematic

The main components our facility setup is made off are the following:

- two identical plenum;
- four vertical riser tubes of the length of $\sim$ 2 m (78 in equals 1.98 m);
- four vertical downcomer tubes of the length of $\sim$ 1.83 m (72 in);
- four pulse heater tubes of the length of $\sim$ 0.41 m (16 in);
- four flexible metal tubes of the length of $\sim$ 0.61 m (24 in);

Specifically, each vertical riser tube has a pulse heater tube at its lower end, because the

Thermal Time-of-Flight (TToF) sensors, which will be discussed in details in the next chapter, measure the gas velocity at the riser tubes inlets. Moreover, each downcomer tube has a flexible metal tube at its upper end. This solution is intended to consider the different thermal expansion at which riser tubes and downcomer tubes are exposed, because of different heating rates.

The technical drawing of the two identical plena is shown in the next image.

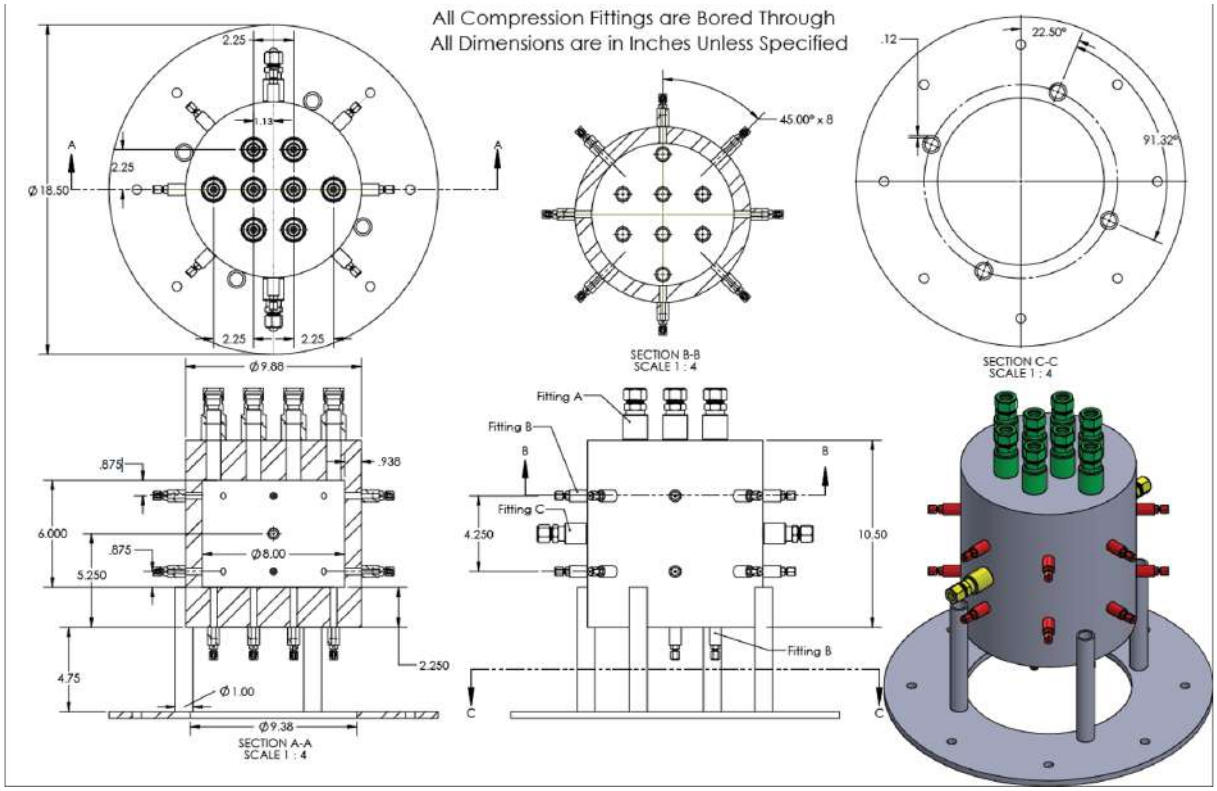

Figure 2.2: Plenum schematic

Each plenum has a diameter of ~ 0.24 m (9.38 in) but the total footprint is ~ 0.47 m, as the support base must also be considered. Each tube is horizontally spaced from the next one by ~ 0.057 m.

It is important to underline that the four tubes arranged in the same horizontal line are the riser tubes, as the downcomer tubes are placed toward the outside of the cylinder.

As it can be seen from the previous image, each plenum has 24 spots for thermocouples; 16 are horizontally inserted into the plenum, divided into two groups of 8 thermocouples each

arranged on two different levels. The remaining 8 thermocouples are vertically inserted in the plenum, from the bottom upward in the case of lower plenum and from the top downward in the case of upper plenum, in order to measure the temperature at the inlet and outlet of each tube, respectively.

The next two images are intended to help understanding the radial and axial positioning of thermocouples.

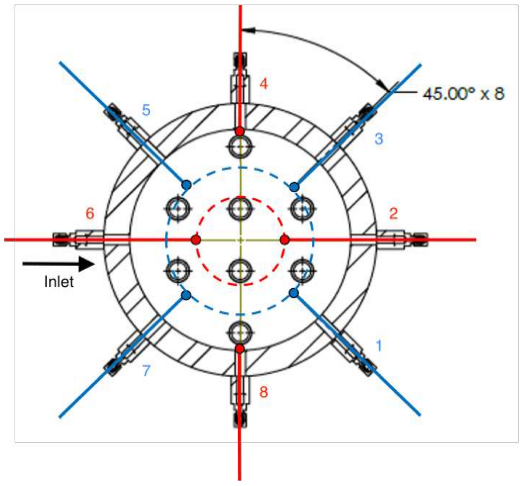

Figure 2.3: Radial thermocouples' placing

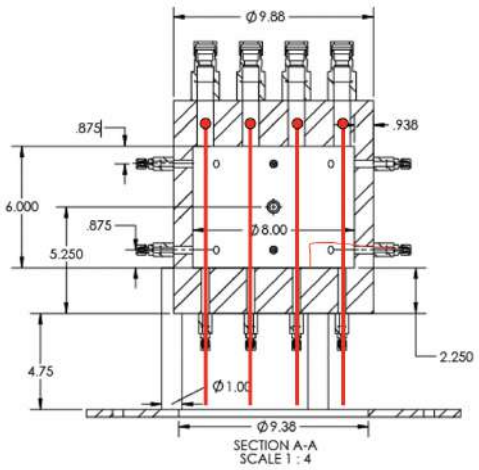

Figure 2.4: Vertical thermocouples' placing

In order to better understand the temperature profile within each plenum, two radial locations are investigated, as illustrated in Figure 2.3. Moreover, it has to be mentioned that only 6 thermocouples are installed at each level because the remaining two would interfere with the external riser tubes.

In accordance with what the reactor's manufacturer suggested, K-type thermocouples have been used. Type K thermocouple refers to any temperature sensor containing Chromel (alloy made up of mainly nickel and chromium plus nine other elements) and Alumel (alloy made up of nickel, manganese, aluminum, silicon and nine other elements) conductors, where Chromel is the positive wire and Alumel is the negative one, that meets the output requirements as stated in ANSI/ASTM E230 or IEC 60584 for Type K thermocouples. All thermocouples were purchased from Omega Engineering, and, among the others, KQXL-18U-6 model was the best option for experimental conditions. The model

has a diameter of 3.18×10^{-3} m, a probe length of 0.15 m and it is rated up to 1150 °C. Moreover, this model has an ungrounded junction, meaning that the two wires welded together do not touch the metal sheath, as they are isolated using a non-conductive powder, such as magnesium oxide. A side effect of the presence of this material is a slower thermal response from the media being measured and in turn it affects the response time of the instrument. Lastly, two thermocouples have been spot-welded on each tube at two different vertical positions. The lowest, which in the following will be referred to as Wall Thermocouple Lower Level (WL) is placed at, while the other one, which will be referred to as Wall Thermocouple Upper Level (WU) is placed at

Nine eight-channels thermocouple/voltage input USB Data Acquisition Modules (DAQs) from Omega Engineering are installed in the facility. The OM-USB-TC module provides eight differential thermocouple input channels and has two integrated cold junction compensation (CJC) sensors for thermocouple measurements. The Data Acquisition Modules are software programmable, and the recording and elaboration of thermocouple signals has been done using LabVIEW.

Each riser tube and downcomer tube is provided with a heating coil, where a resistive conductor generates heat when an electrical current flows through it. Specifically, each heating coil has a length of 7 m, and both cold leads are 1.25 m long. The heating coil contains a sheath made of Inconel 600, an alloy of nickel and chromium and its main function is to protect the heating element from corrosion and more importantly in this case from high temperatures. Lastly, the manufacturer indicates a specific resistivity of 6.30 ohm/m, which refers to the resistance the heating element material offers to the flow of electrical current. Each heating coil is wrapped around a tube with a total of approximately 65 to 70 rounds, in order to have a uniform distribution of temperature on the external surface. In the following image it is shown how the heating coils were installed in the riser tubes.

Figure 2.5: Heating coil on riser tubes

Each heating coil on the riser tubes is connected to a single variac, while those on the downcomer tubes are connected in pairs to two different variacs.

By definition, a variac, also know as a variable autotransformer or variable transformer, is an electrical device used to vary the output voltage of an AC power source, by adjusting the turns ratio between the primary and secondary windings, the first being connected to the input voltage source and the second being connected to the load. These devices are commonly used among industries, because they can provide precise control of output voltage. All of them are rated up to 200 V.

Pressure within the system is measured using a pressure transducer purchased by Omega Engineering. The chosen model (PX109-1KG5V) is rated from 0 up to 6.90×10^6 Pa (equivalently from o up to 1000 psi), with a nominal accuracy of 0.5% BFSL (BFSL stands for Best Fit Straight Line, and it represents the maximum deviation from a best-fit straight line that represents the sensor's output over the specified pressure range). This model is equipped with a piezoresistive ceramic diaphragm as sensing element. When pressure

varies in the system, the diaphragm undergoes mechanical deformation and because of the nature of the sensing element, in turn it changes its electrical resistance. The piezoresistive ceramic material is part of a Wheatstone bridge circuit and its change in electrical resistance causes an imbalance in the circuit, from which a small electric current is generated and subsequently amplified in order to obtain a stronger detectable output electrical signal. Lastly, signal processing and temperature compensation are applied for obtaining a better accuracy on the pressure measurement. The output signal of the instrument (4 to 20 mA or 0 to 5 V) is then elaborated by a dedicated DAQ module. The pressure transducer is placed in the lower plenum through a dedicated inlet.

For the success of the experiment, it is of paramount importance to thermally insulate the system. For this purpose, fiberglass insulation sheets have been used and in the first stage of the experiment they have been placed around the riser tubes only. The thermal insulation is rated up to $\sim 540\,^{\circ}\mathrm{C}$ and characterized by a heat flow rate of ~ 274 J at ambient temperature. Each sheet has a thickness of 3.81×10^{-2} m and a R value of 5.8, that is the thermal resistance of the material, a measure of how much a material is effective in resisting to a heat flow.

In the following image, the thermal insulation placing schematic is shown.

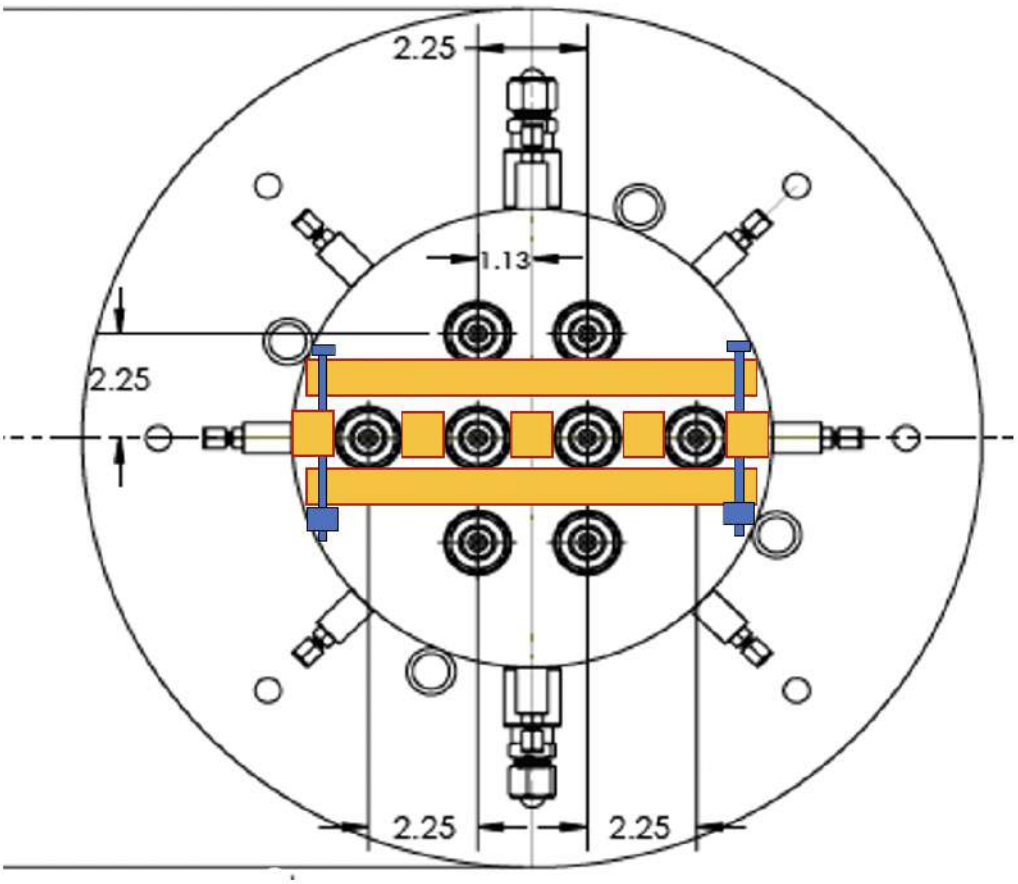

Figure 2.6: Thermal insulation placing

Gas is provided to the tank using a gas tank, connected to the facility setup through a series of pipes and fittings. At the reactor inlet, a three-way valve is used: one way is the inlet to the valve, the second one is the inlet to the reactor, while the third connects the supply line to building vacuum line, which is used for removing the hot gas at the end of each experiment or to provide a certain degree of vacuum at the beginning of the experiment, as it is preferable to remove any trace of air before starting the collection of data, because it would affect the physical and chemical properties of the primary gas.

The following images are intended to help in better understanding the system as a whole.

Figure 2.7: Plenum

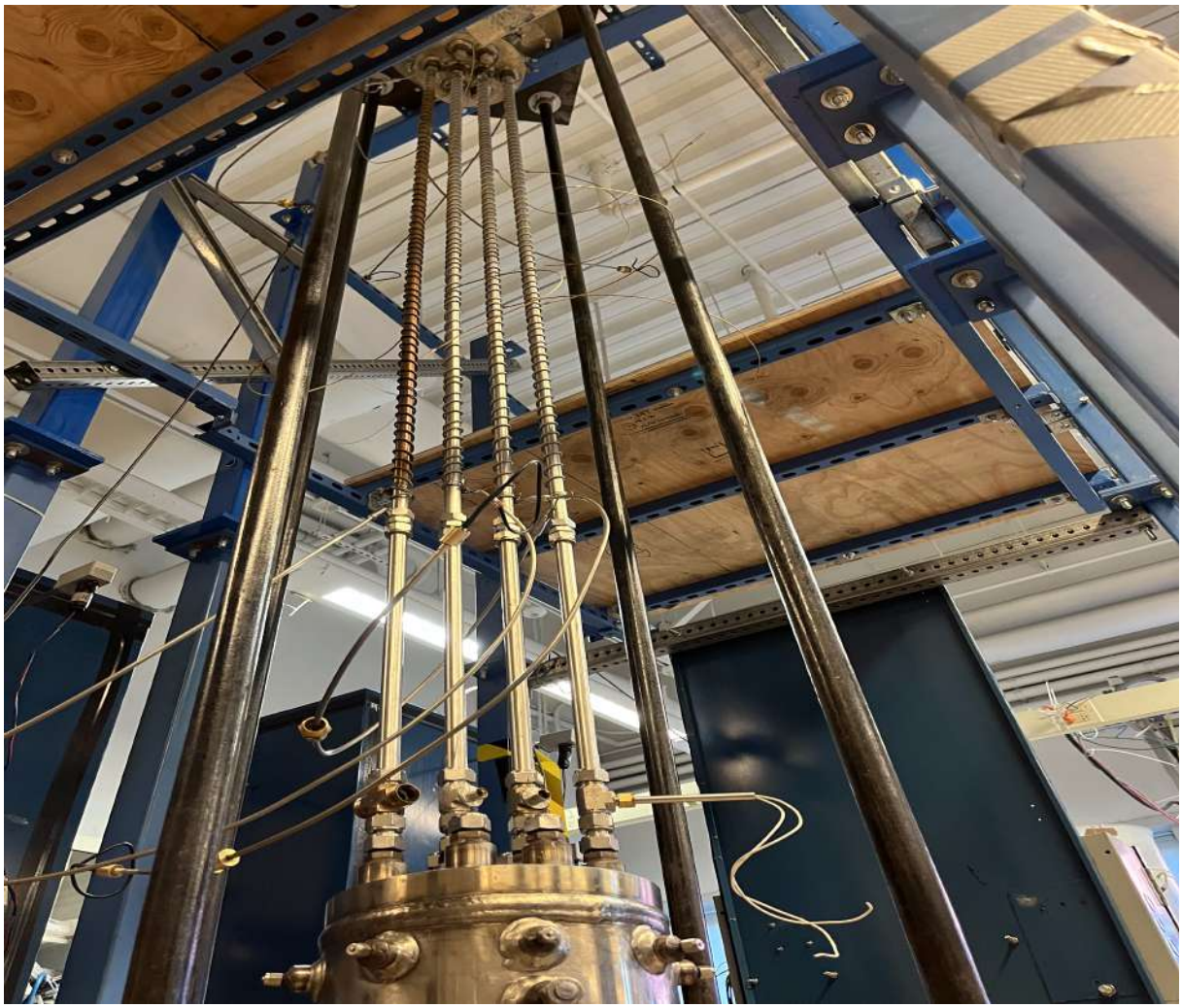

Figure 2.8: Riser tubes

In Figure 2.8, lower and upper plenum are connected through the four riser tubes, on which the heating coils are already installed. This picture was taken in a preliminary design phase: in fact, the instrumentation section for the thermal time of flight sensor is in the old design and therefore it should not draw attention in this picture, the intent of which is to show the vertical extension of the natural circulation loop.

Figure 2.9: Complete setup

Figure 2.9 shows the complete natural circulation loop as a whole. It is not possible to see the riser tubes, which are wrapped by the thermal insulation, while it is possible to note the downcomer tubes in the external radial position. Upper and lower plenum are wrapped by the thermal insulation as well.

Chapter 3

Thermal Time of Flight (TToF)

3.1 Introduction

Flow velocity measurement is an essential aspect of various industries such as oil and gas, chemical processing, power generation, and HVAC, among others. Accurate measurement of gas flow velocity is critical for optimizing processes, controlling system performance, ensuring safety, and reducing costs. Conventional flow measurement techniques involve the use of devices such as differential pressure meters, positive displacement meters, and turbine meters, among others.

Firstly, the difference between a *flow switch* and a *flow sensor* must be defined. A *flow switch* is a device designed to make and break an electric current in a circuit. Two distinct actions can be performed: closing its contacts and turning a specific piece of equipment ON, or opening its contacts and turning a specific piece of equipment OFF. Flow switches are commonly used for basic measurements, either for determining whether a fluid is flowing in the system or for controlling if an imposed flow rate is reached. A *flow sensor*, also known as *flow-meter*, is a device used in measuring how much fluid is passing through a certain section in the unit of time. In the following, reference will be made only to flow-meters.

Generally, most of the measuring devices estimate the flow rate by either calculating the fluid's velocity or the change in its kinetic energy. Fluid velocity can be easily related to the volumetric flow rate by means of the following basic relationship:

$$Q = A \cdot v \tag{3.1}$$

where Q is the volumetric flow rate, A is the cross-sectional area and v the velocity. Other factors, such as fluid viscosity and density, as well as friction with the tube, affect the fluid velocity, but Eq. 3.1 gives a sufficiently accurate indication of the flow rate. While these devices have been widely used for many years, they have several limitations, including the need for re-calibration, sensitivity to fluid properties such as temperature and pressure, and high maintenance costs.

For these reasons, in recent years innovative solutions have been investigated. Among them, thermal flow-meters are an interesting solution for measuring gas velocities within pipes. Normally, these devices rely on two different principles; in fact, they can either introduce a known amount of heat into the flowing stream and measure a temperature gradient or maintain a probe at a specified temperature and calculate the energy required to do so.

Nowadays, three distinct thermal flow meter configurations are available in the market; these are: anemometers, calorimetric sensors, and thermal time-of-flight sensors.

An *anemometer* is commonly a hot-wire sensor, where the latter acts as both heating element and temperature sensor. The working principle used for measuring the fluid velocity is to calculate the amount of heat which is taken away from a heated surface by the flowing fluid. The main disadvantage in using these devices is related to frequent surface contamination of the heating element.

A *calorimetric flow meter*, instead, is made up of a heating element and two temperature sensors, one upstream and one downstream the heater. The temperature profile in the heater region is then associated to the flow rate. These devices are mainly used for low

velocity applications, but they present limitations due to the need for a large temperature difference between the two temperature sensors and because they have a limited linearity range.

Lastly, *thermal time-of-flight sensors* are a promising technology in the measurement field. The physical phenomenon on which this technology is based is relatively simple: the fluid velocity is directly related to the time it takes for a heat pulse to travel a known distance. Consequently, a thermal time-of-flight sensor is generally made up of a heating element and two or three downstream thermocouples. As reported by Mahvi et al.[10], several authors have designed and tested thermal time-of-flight sensors for liquids, especially using low velocities, since the sensor has a slow response time. As reported by Ashauer et al.[3], a reasonable range of operating conditions for these sensors is between 1.00×10^{-3} and 1.50 $\mathrm{m\,s^{-1}}$, but it has to be mentioned that uncertainties were either large or not reported.

Several authors have reported that this type of sensor should be exempt from calibration [3],[7],[8],[10]. However, since our time-of-flight sensors are handcrafted and not assembled with precision tools, a calibration process was needed for each one. In fact, the positioning of both heating element and thermocouples' sensing elements is crucial, especially considering a laminar flow regime, characterized by the well-known parabolic velocity profile.

This study aims to develop a flow velocity measurement device for installation in the high-temperature (up to 700 °C) and high-pressure (up to 70 bar) experimental facility at the City College of New York, to study natural circulation flows in the experimental setup which aims to represent the behavior of a General Atomics' MHTGR 350 MWt.

3.2 Methodology

The experimental setup consists of a test section connected to a gas supply tank via a flowmeter. A simplified layout of the experiment and the actual experimental pipe

with heating element are shown in the following images. In order to reduce the image dimension, the third thermocouple in the schematic is not shown.

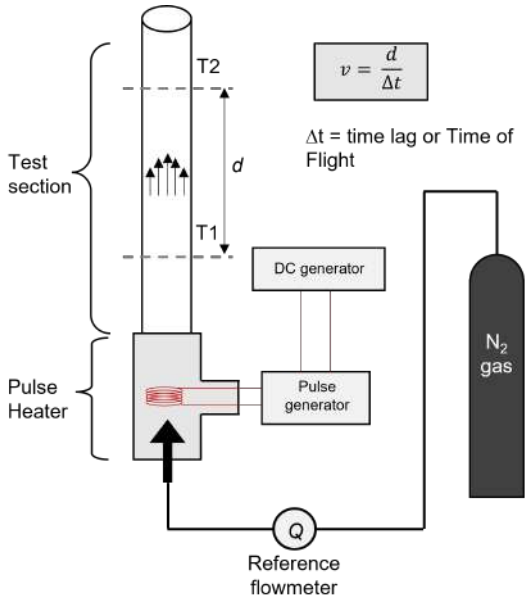

Figure 3.1: Setup schematic

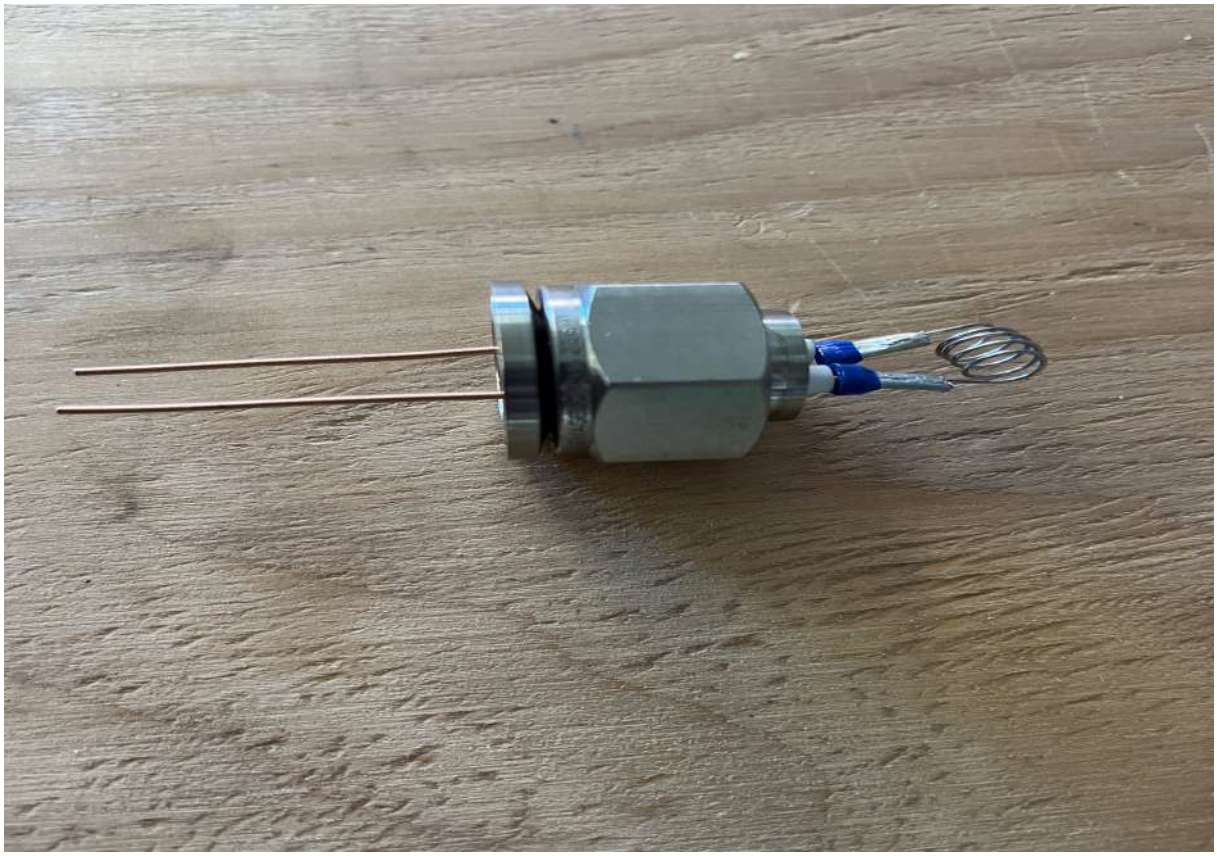

Figure 3.2: Heating element

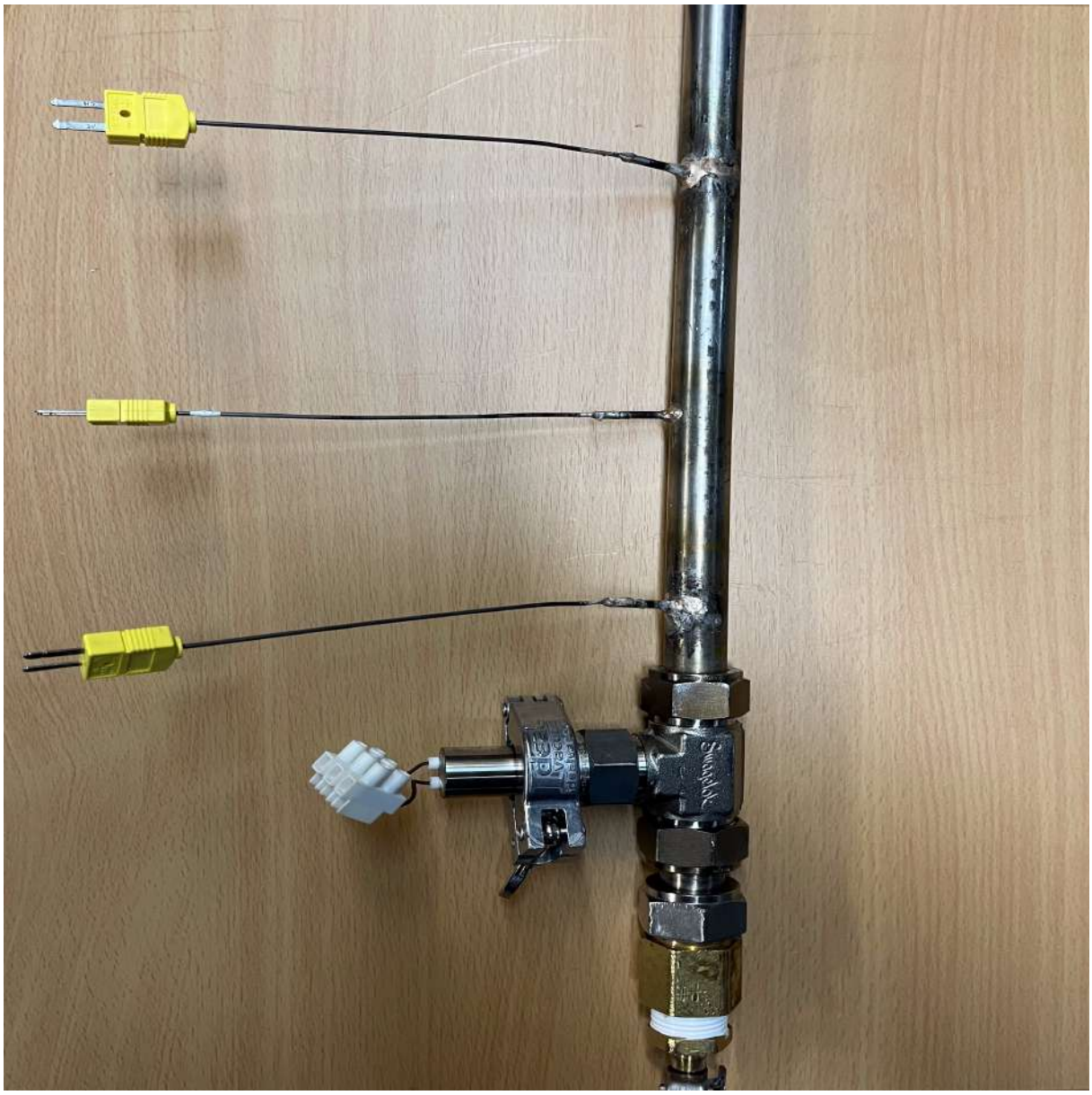

Figure 3.3: Test tube

Nitrogen gas is supplied to the test section at atmospheric pressure and room temperature after passing through a reference flowmeter. The test section consist of a 1.27×10^{-2} m ID straight pipe, 4.57×10^{-1} m in length, with three thermocouples into the tube to measure the temperature of the flowing gas. Thermocouples 1 and 2 are 7.62×10^{-2} m apart (3 in), while the second and third are 1.02×10^{-1} m from each other (4 in). Moreover, the first thermocouple is 2.56×10^{-2} m above the heating section. The pulse heater is a helical coil of NiChrome wire, 5.00×10^{-4} m in wire diameter, and 1.00×10^{-2} m of coil diameter, with a total of 7 turns, it is mounted of a QF16 flange, using a O-ring and a clamp to

complete the heating section and it is rated up to 1 kW and 25 A. It is connected to the 18 ft long pipe through a stainless-steel Swagelok union tee. The pulse heater is controlled by a pulse generator and is powered by a DC generator. A maximum pulse power of 50 W is supplied into the heater. The pulse has a rectangular shape, the width is set to be 1.00×10^{-1} s with 5 s time period between consecutive pulses. For the generation of the pulse signal, a cycle delay drive module has been used. The device from PEMENOL, rated from 3.3 V up to 30 V with a maximum output current of 8 A, allowed to impose the desired experimental conditions.

Three K-type thermocouples are used for measuring the flowing gas temperature. They have 1.59×10^{-3} m diameter, and have an exposed junction for faster response time. The exposed junction is located at the center line of the test section. The thermocouples are connected to a National Instruments data acquisition module and the temperature measurements are recorded at 100 Hz. The thermocouples have an uncertainty in measurement of $\pm 0.5\,^{\circ}\mathrm{C}$.

3.3 Governing Equations

Three different governing equations can be written to analytically describe the system; these are: Navier-Stokes equation for momentum conservation, the energy equation and the Joule heating equation. All of them are reported in the following.

$$\rho \frac{\partial \mathbf{v}}{\partial t} + \rho \cdot \mathbf{v} \cdot \nabla \mathbf{v} - \mathbf{F} = \nabla \cdot [-p\mathbf{I} + \eta(\nabla \mathbf{v} + (\nabla \mathbf{v})^T] \tag{3.2}$$

where $\mathbf{F}$ is a body force term in $\mathrm{N}{\cdot}m^{-3}$, ρ the density of the fluid in $\mathrm{kg}{\cdot}m^{-3}$, $\mathbf{v}$ the velocity in $\mathrm{m}{\cdot}s^{-1}$, η the dynamic viscosity in $\mathrm{N}{\cdot}\mathrm{s}{\cdot}m^{-2}$ and p the pressure in $\mathrm{N}{\cdot}m^{-2}$. In Equation 3.2, the first two terms corresponds to the investigated volume inertia, $\mathbf{F}$ the external forces, $\mathrm{p}{\cdot}\mathbf{I}$ the pressure and the last term the friction.

$$\nabla \mathbf{v} = 0 \tag{3.3}$$

where Equation 3.3 gives the boundary condition by constant density ρ

$$\rho \cdot c_p \frac{\partial T}{\partial t} + \nabla \cdot (-\lambda \nabla T) = Q - \rho \cdot c_p \cdot \mathbf{v} \cdot \nabla T \tag{3.4}$$

where T is the temperature in K, λ the specific thermal conductivity in $\mathrm{W}{\cdot}m^{-1}{\cdot}K^{-1}$, c_p the specific heat capacity of the fluid at constant pressure in $\mathrm{J}{\cdot}kg^{-1}{\cdot}K^{-1}$ and Q the heat source in $\mathrm{W}{\cdot}m^{-3}$.

$$-\nabla \cdot (\sigma \nabla V - J^e) = Q_j \tag{3.5}$$

where this last equation describes the joule heating in the Nichrome wire where the electrical energy supplied by the DC generator in converted in thermal energy. In particular, σ is the electrical conductivity in $m^{-1}{\cdot}\Omega^{-1}$, V the electrical potential in V, J_e the externally generated current density in $\mathrm{A}{\cdot}m^{-2}$, and Q_j the current source in $\mathrm{A}{\cdot}m^{-3}$.

For solving this set of equations, it would also be necessary to initiate some of the parameters, because some of them depend on the velocity, others on the temperature. To sum up, solving the system of equations would require the use of a specific software for multiphysic simulations, such as COMSOL multiphysic, the use of which, however, requires specific skills and experience.

3.4 Data Processing

The temperature data collected from the Thermal Time of Flight sensor are processed using MATLAB. The temperature time series data is imported and the outliers are removed. The temperature data is then normalized to have the maximum and minimum at 1 and 0, respectively. The normalized temperature data obtained from the thermocouples is shown in Figure 3.2 for demonstration.

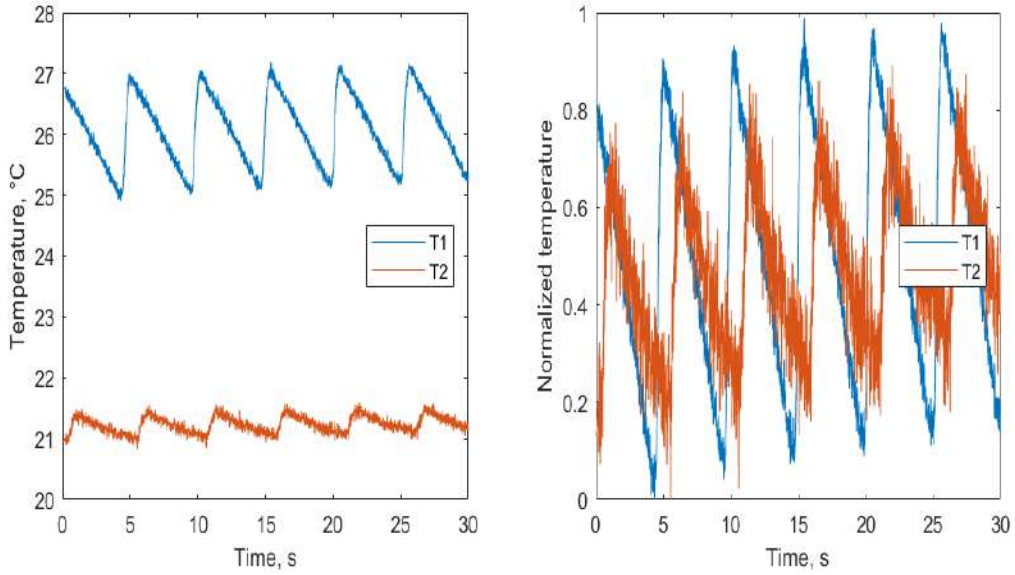

Figure 3.4: Raw and normalized temperature measurement

To calculate the time of flight of the temperature pulse to travel between the three temperature measurement points, a cross-correlation method is implemented. Cross-correlation works by sliding one signal across another for a given time lag and comparing the two signals at each time lag. At each step, the similarity between the two signals is calculated using correlation coefficient, and the time lag at which the correlation is the highest is determined to be the time of flight.

In the experiments, a cross-correlation was applied over 300 s of temperature data. The flowrate was kept constant over these 300 s and this was verified from the reference flowmeter. A maximum flowrate of $1.57 \times 10^{-4} \mathrm{m}^3\,\mathrm{s}^{-1}$. In this condition, the Reynolds number is well below 2000, meaning that the flow should be considered as laminar. However, the test section has a short development length, thereby making it inconclusive to determine whether the flow is in the laminar or turbulent flow regime. Lastly, it has to be mentioned that the experimental setup entrance region length is similar to the one in the natural circulation loop, where the instrumentation tube is going to be deployed.

In the following images, the MATLAB code that has been used for elaborating the temperature data series is shown.

```
clear all; clc;

%import of the LabVIEW file with extension .lvm
TEST = lvm_import('temp_2cfh');

Column_names = TEST.Segment1.column_labels;
T = array2table(TEST.Segment1.data,'Variablenames'...
    ,Column_names);
T = renamevars(T,'X_Value','time');
%temperature data series import
t = T.time; dt = median(diff(t));
T1 = T.Temp3;
T2 = T.Temp2;
T3 = T.Temp1;

% Remove and replace outliers
fillmethod = 'spline';
findmethod = 'median';
T1 = filloutliers(T1,fillmethod,'movmedian',1);
T2 = filloutliers(T2,fillmethod,findmethod);
T3 = filloutliers(T3,fillmethod,findmethod,1);
n_avg = 10; %sliding window for the average
%temperature average
T1 = movmean(T1,n_avg);
T2 = movmean(T2,n_avg);
T3 = movmean(T3,n_avg);
%temperature normalization
T1_n = (T1 - min(T1))./(max(T1) - min(T1));
T2_n = (T2 - min(T2))./(max(T2) - min(T2));
T3_n = (T3 - min(T3))./(max(T3) - min(T3));
```

```
%cross-correlation
[r,lags] = xcorr(T2_n,T1_n,round(1/dt), 'unbiased');
r(lags == 0) = NaN;
[R12,I] = max(r);
Tof_corr12 = dt*lags(I);
figure(2);
plot(dt*lags,r); grid on;
hold on;

[r,lags] = xcorr(T3_n,T1_n,round(1/dt), 'unbiased');
r(lags == 0) = NaN;
[R13,I] = max(r);
Tof_corr13 = dt*lags(I);
figure(2);
plot(dt*lags,r); grid on;
hold on;

[r,lags] = xcorr(T3_n,T2_n,round(1/dt), 'unbiased');
r(lags == 0) = NaN;
[R23,I] = max(r);
Tof_corr23 = dt*lags(I);
figure(2);
plot(dt*lags,r); grid on;
hold on;
```

Figure 3.5: TToF MATLAB code

Specifically, the function lvm_import is used for importing the LabVIEW file with extension .lvm into the MATLAB environment. Moreover, the *filloutliers* function is used in order to find and replace outliers in a data set. According to MATLAB, an outlier is an element that is greater than 3 scaled median absolute deviation away from the median. For correctly using this function, two important parameters have to be defined. *findmethod* specifies the method to determine outliers, while *fillmethod* specifies how the outliers have to be replaced. In this case, 'median' and 'spline' have been used for *findmethod* and *fillmethod*, respectively. It means that each value greater than 3 scaled median absolute deviation away from the median is considered an outlier and a piecewise cubic spline interpolation of non-outlier entries is used for replacing them. Lastly, the *xcorr* function

has been used for calculating the cross-correlation between time series. In particular, a cross-correlation is calculated for each pair of temperature data set, in order to find out which pair of data are in better agreement.

3.5 Calibration results

In this section, the most important results of the calibration process are presented.

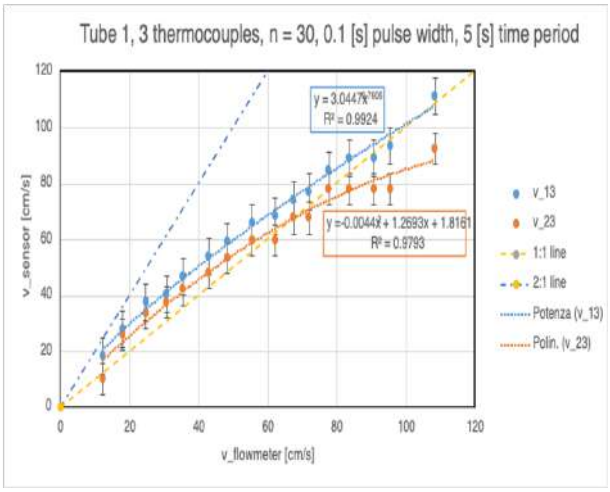

Figure 3.6: Tube 1 calibration curves

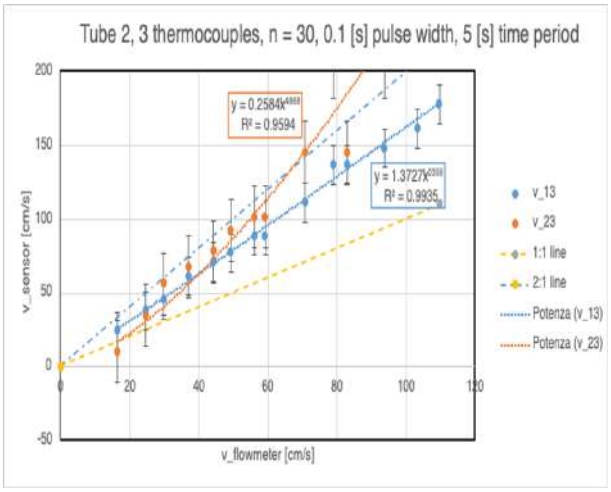

Figure 3.7: Tube 2 calibration curves

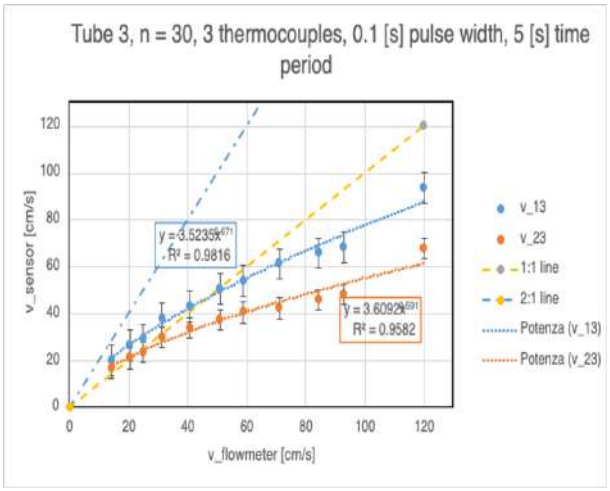

Figure 3.8: Tube 3 calibration curves

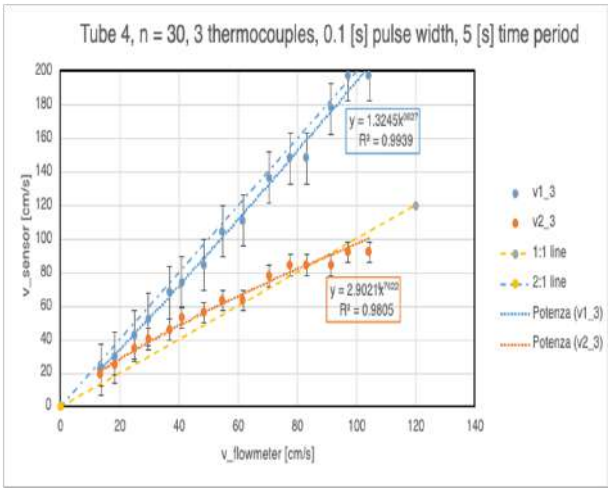

Figure 3.9: Tube 4 calibration curves

First of all, two different values of velocity are calculated for each tube: v_{13} indicates the velocity calculated between thermocouples 1 and 3, while v_{23} the one between thermocouples 2 and 3. v_{12} is not reported because experimental data were random and then not

significant. This could be due to the fact that both thermocouples 1 and 2 are relatively close to the pulse heater section and for this reason the signal being measured is affected by noise. As a result, it was difficult to implement the cross-correlation between these two sets of temperature data. In each graph, the 1:1 line represents the case in which flow meter and flow sensor measure the same velocity, while the 2:1 line the case in which the flow sensor measures a velocity that is the double of the one measured by the flow meter. This is done because of the parabolic profile of the velocity in laminar flow regime; in fact, if both thermocouples' sensing elements are perfectly at the center line, the maximum velocity is measured, which corresponds to the double of the mean velocity that can be obtained from the flow meter. Considering this option stems from the fact that the thermocouple sensing element radial position is not certain, as the instrumentation tube is handcrafted, and it is reasonable to assume that during the welding process the thermocouples placing turned out to be slightly different from what was originally intended. In addition, also the regression curves with their equations are reported.

There are a few more reasons to explain why the time-of-flight sensor does not give very accurate measurements of the fluid velocity. First of all, by simply applying the definition of Reynolds number, a laminar flow region would be expected. However, it is reasonable to think that the flow is not fully developed in the instrumentation tube, since both the heating section and the thermocouples are relatively close to the inlet of the instrumentation tube. Moreover, this also applies in the natural circulation loop, as the time-of-flight sensors are placed at the outlet of the lower plenum and then the velocity profile will be affected by the paths the gas has to take. Secondly, both the heating element and the thermocouples affect the path of the flowing fluid, and it is reasonable to assume that slight turbulence or deviations to the path are introduced in the flow. Additionally, even if each test tube has been thermally insulated with a layer of fiberglass insulation, a certain amount of heat is lost to the environment, and this loss affects the accuracy of the sensor, since its working principle lies precisely in the heat transfer from a heat source to a few sensing elements. Last but not least, when the fluid flows on the hot wire, locally its temperature suddenly increases, and it could lead to a slight expansion

of the gas. It means that the gas moves because of its velocity but also because of the thermal expansion in the axial direction, and thus the time elapsed to travel a certain distance decreases, resulting in higher gas velocity.

Chapter 4

Natural Circulation

4.1 Introduction

Natural circulation is the circulation of a working fluid in either a closed loop or open loop caused by density changes in the fluid induced by temperature gradients. In general, a natural circulation loop is made up of a heat source, a heat sink and a set of connecting pipes [1]. In a nuclear reactor plant, the heat source is represented by the *reactor core* while the heat sink by the *steam generator*, and they are connected in a continuous way by the set of pipes. One of the most interesting aspects of natural circulation is that it can set to steady state conditions and continue indefinitely, if heat source and heat sink are maintained at constant temperature and if the loop is kept constant, respectively. The fluid circulation is the result of buoyancy forces, due to variations in fluid density when it is exposed to different temperatures in the circulation loop. In order to enhance the physical phenomena, the heat sink is generally located above the heat source, and the difference in height can be on the order of tens of meters.

As already introduced in Chapter 1, the most important characteristic of a natural circulation loop is that, being a passive safety system, it does not require any moving parts or externally powered machinery, thus making it a completely independent system that can always be relied on. For this reason, natural circulation loops find several applications in

conventional engineering as well as nuclear industries. As reported by Pilkhwa et al. [12], solar water heaters, transformer cooling, geothermal power extraction, cooling of internal combustion engines, gas turbine blades and nuclear reactor cores. Moreover, natural circulation loops do not require expensive maintenance operations and they are less prone to failures.

Natural circulation loops are already in use in the nuclear energy industry. In fact, it is not uncommon to find natural circulation based steam generators in nuclear plants, especially in *Pressure Water Reactors* (PWRs), *Pressure Heavy Water Reactors* (PHWRs) and *Vodo-Vodyanoi Energetichesky Reaktor* (VVERs). However, natural circulation loops are given increasingly attention for reactor core cooling applications, in particular for decay heat removal during shut-down operations and for core cooling during accident scenarios. In fact, even after the reactor is shut down, a certain amount of heat is still produced by the fission reaction, which will continue to proceed, though with much less rapid kinetics. From the process control point of view, a natural circulation loop is the perfect solution for controlling the decay heat released by the reaction, as no externally powered elements are required, thus reducing costs when the reactor is not in operation. Moreover, natural circulation is also of fundamental importance when it comes to an accident scenario, during which it is reasonable to assume that externally powered machinery are not available and natural circulation becomes the most effective way to remove heat from the reactor core.

The working principle behind a natural circulation loop is very simple; in fact, the working fluid absorbs heat from the heat source, and rejects heat to a colder environment at the heat sink level. The heat transfer process involves temperature gradients for the working fluid, meaning a variation in fluid density which establishes the natural circulation loop in a gravity forces field. The flow is unidirectional and for this reason it is not possible to distinguish a natural circulation loop from a forced one by only looking at the paths the working fluid takes in the system.

Before moving further, it is necessary to present advantages and challenges of natural circulation loops.

First of all, an evident advantage of a natural circulation loop is the elimination of pumps for moving the working fluid, leading to a lower investment capital, as well as lower operating and maintenance costs. Moreover, natural circulation loops are not subject to failures, since no moving parts are present in the loop.

Secondly, NC loops provide a better flow distribution in the large number of vertical parallel tubes commonly used in nuclear reactors. In fact, the use of pumps may introduce flow instabilities and experimental data report that a order of magnitude less in flow instabilities is expected with natural circulation.

Additionally, in natural circulation systems, the flow increases with power, whereas in forced circulation it decreases with increasing power. Thus, natural circulation loops provide a better flow characteristic compared to the one obtained from forced circulation, especially in steam boilers, where the production of steam is far from constant due to power maldistribution.

Also, a natural circulation system is inherently safe from an operational point of view, since it is based on a physical principle and it does not depend on external utilities, the operation of which may suffer of failure.

Lastly, in order to reduce pressure drops along the loop, no elbows or pipe bends are implemented in a natural circulation system, leading to its simple design.

Even though many concept of nuclear reactor are under extensive study and development, such as the *Simplified Boiling Water Reactor* (SBWR), nuclear reactors do not involve NC of the coolant as the primary circulation method. This is mainly due to the challenges that still have to be addressed. The main ones are discussed and analysed in the following.

The main limitation about natural circulation is its intrinsic low driving force, which is a very limiting issue in nuclear reactor, since the reactor core produces a huge amount of thermal energy from the fission reaction. The only way to increase the driving force is by increasing the loop height, which in turn may be expensive and lead to a structural

instability.

Because of the low driving force and the need of high flow rates, pressure drops along the loop must be limited. There are three main solutions to this limitation; these are: use of large diameters, simplifying the system and the elimination of components. Using large diameters is the easiest way to reduce pressure drops, but at the same time the system volume increases, that is both uneconomical and may introduce safety-related issues. Both the elimination of elbows, connections and components are viable solutions, even if in some cases difficult to implement.

Another limitation of a natural circulation loop is its intrinsic flow instability. Even though also forced loops present a similar problem, natural circulation loops highly depend on the driving force, which affect the flow rate and the latter in turn affect the driving force. As a result, in certain operating conditions, it is reasonable to expect flow oscillations.

Additionally, it is crucial to define start-up and operating procedures. In fact, natural circulation loops present instabilities in low pressure conditions, which take place during reactor startup. Also, increasing power and pressure can lead to a premature *Critical Heat Flux* (CHF) condition, meaning that the heat flux on the surface of the fuel deteriorates. As a result, a precise procedure must be defined ahead of reactor operation.

4.2 State of the art

Natural circulation loops have been given increasing attention over the past decades and as a result, many experimental investigations are present in the literature. A brief overview of the work that has been accomplished so far is given in the following.

Said et al. [13], [14] conducted an investigation on natural convection heat transfer in a unique scaled-down dual-channel facility, made up of upper and lower plena connected by only two channels, one riser tube and one downcomer tube. The attention is focused on the effect of upper and lower plenum and channels temperature on natural circulation heat transfer efficiency during an accident scenario of *Pressurized Conduction Cooldown*

(PCC) in a *Prismatic Modular Reactor* (PMR). The set of experiments is conducted using air as working fluid and at a pressure of 413.7 kPa, or equivalently 4.137 bar. Thanks to the use of advanced fast response flush mounted heat transfer sensors and several temperature sensors on the outer surface of the 1 m long tubes, they monitored several parameters, such as the air centerline temperature, the inner surface temperature, the local heat transfer coefficient and the local Nusselt number, and plotted them as a function of the non-dimensional length. At the end of the study, they concluded that first of all the majority of heat removal occurs in the upper plenum

4.3 Preliminary Experiments

The experimental facility in the *Thermofluids Laboratory* at *The City College of New York* is, to the best of our knowledge, among the most sophisticated and advanced natural circulation loops in the research field.

In fact, the facility setup there is much more complex than the ones reported in the previous paragraph. It consists of four riser tubes and four downcomer tubes, connecting the upper and the lower plena. The use of multiple riser and downcomer tubes lies in the fact that in this way it is possible to investigate upward, downward and stagnant flow distributions between parallel flow passages, giving important information about the flow characteristics in the natural circulation loop.

Moreover, our experimental facility works with much more demanding operating conditions, in terms of both temperature and pressure. In fact, experiments are performed for a wide range of temperatures and pressures, up to 750 °C and 70 bar, to simulate plenum to plenum gas dynamics under both *Pressurized Conduction Cooldown* and *Depressurized Conduction Cooldown* events. Especially in terms of working pressure our system is a step forward with respect to other facilities reported in the literature.

Additionally, most of the previous works are conducted using air as working fluid, whereas in our facility nitrogen was used and helium will be used for future experiments. Using

nitrogen gas and especially helium gas allows a better representation of the natural circulation phenomena, closer to what is expected to happen in a real nuclear reactor.

Before discussing the natural circulation experiments, it is important to present the results of some preliminary work that was done. In particular, pressure leak test and heat loss tests will be reported and discussed in the following.

The *pressure leak test* consists in pressurizing the reactor to a set value and record how pressure varies over time. A reduction of system pressure is expected, as the gas leaks from the numerous connections used in the setup. A solution of water and soap was used for detecting leaks; in fact, spreading the solution over the leaky connections makes it easy to detect them, as soap bubbles form in their presence.

In the following, pressure leak tests with both nitrogen and helium are reported.

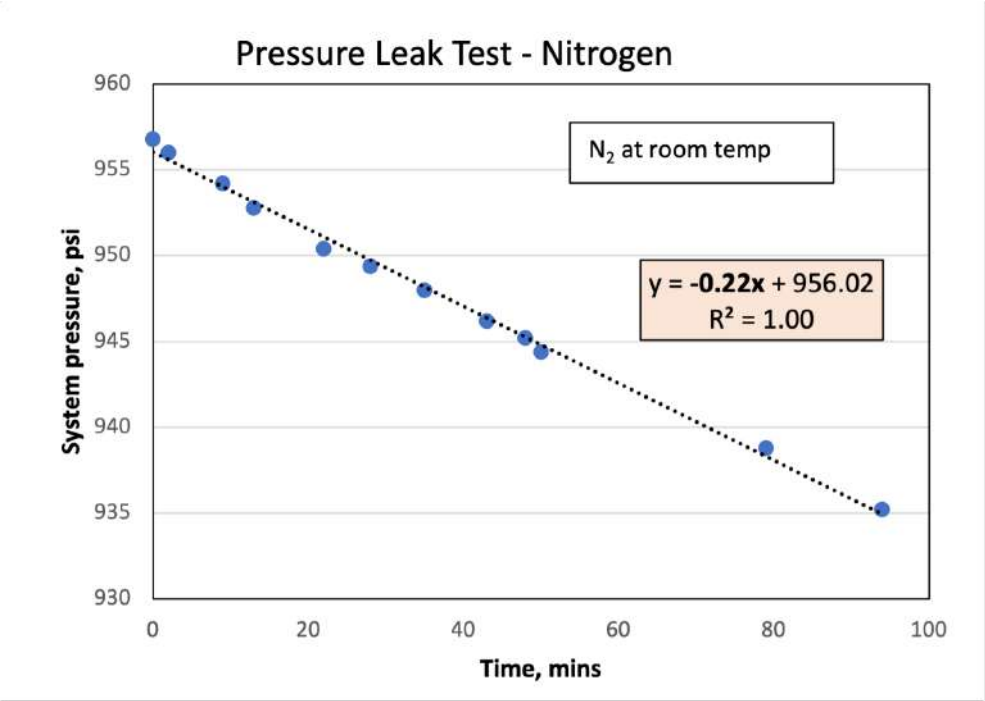

Figure 4.1: Pressure Leak Test with Nitrogen gas

The pressure leak test with nitrogen gas was conducted for a period of approximately 100 min, with an initial value of pressure slightly below 66 bar (or equivalently 955 psi). This value is very close to the maximum value of pressure the system is rated for. As it can be

seen from Figure 4.1, over the first 100 min it is reasonable to assume that the pressure leaks follow a linear relationship, as indicated by the regression curve. The pressure loss rate corresponds to 1.52×10^{-2} bar/min or 9.10×10^{-1} psih^{-1}. This result is extremely satisfactory, as pressure leaks are almost negligible.

There are several reasons behind the choice of nitrogen as one of the gas used for the pressure leak test. First of all, it is one of the gases used for the natural circulation experiments. Secondly, it is cheap, physically and chemically stable, and lastly it has a low solubility, meaning that it has a low tendency to be absorbed or diffuse through sealing materials or system walls.

In the following, pressure leak test using helium gas is shown.

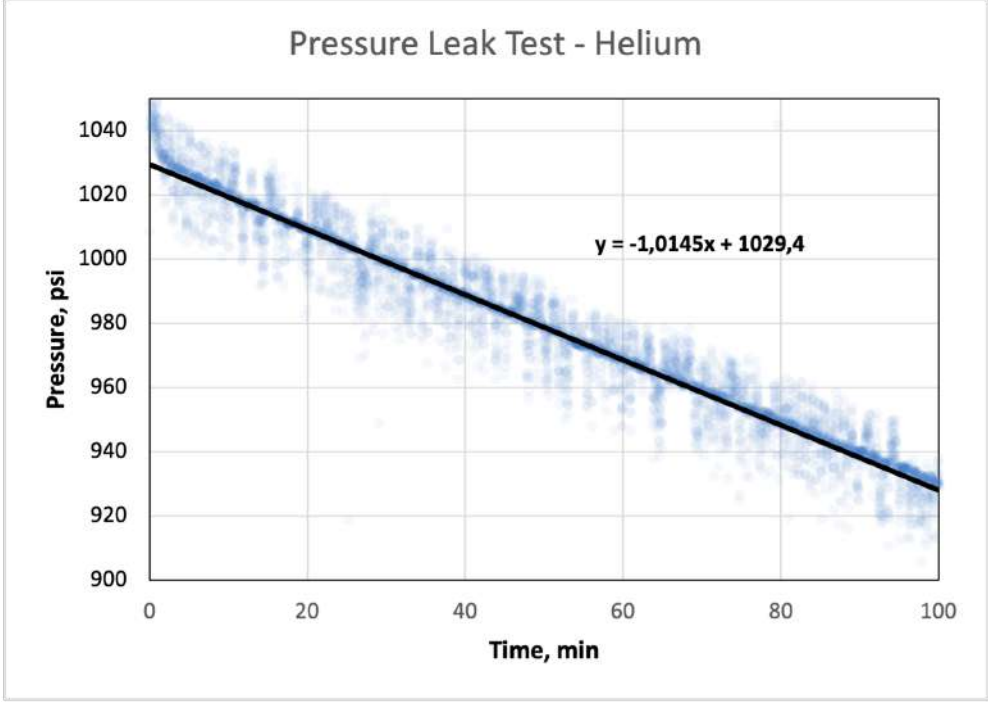

Figure 4.2: Pressure Leak Test Helium

For the Helium pressure leak test, an averaging function was used in order to remove the noise from the pressure transducer signal.

The initial pressure for the helium pressure leak test was slightly higher than the one for the nitrogen pressure leak test, being approximately 72 bar (or equivalently 1050 psi).

Also, the pressure leak rate is higher in the helium experiment, being approximately 6.89×10^{-2} bar min^{-1} or equivalently 4.14 psi h^{-1}. This result should not surprise; in fact, helium has a lower molecular density, resulting in higher tendency of its molecules to diffuse and escape from small leaks. For this reason, the first pressure leak test was conducted using nitrogen, since it is easier to detect where its molecules leak from. Moreover, helium has a high tendency to diffuse, meaning that a certain amount of the gas is expected to diffuse in the sealing material. However, the result obtained from the helium pressure leak test was satisfactory, because it is necessary to take in consideration that a certain escape rate can not be avoided, since perfect sealing is not attainable.

Another important test carried out before those on natural circulation was the heat loss test.

A *Heat Loss Test* is a procedure conducted in order to determine the rate of heat lost in a system. It was necessary for our heat transfer studies, as discussed in the following sections. It was useful for identifying areas with higher heat losses and evaluating the thermal insulation effectiveness.

The experiment is conducted under vacuum conditions; in fact, it is necessary that no gas is present within the system, as it would remove a certain amount of heat. For this reason, the experimental setup was connected to the building vacuum line for approximately 30 min before the experiment was conducted.

All four riser and downcomer tubes were heated up at the same time during the experiment and the latter was performed till reaching a steady-state value of temperature for each tube. In this condition, the heat supplied by the variacs equals the heat loss to the environment, giving the heat loss rate.

Before showing the heat loss test results, it is important to remember that each vertical tube has two thermocouples spot-welded on the outer surface. For this reason, it is possible to schematically identify two different sections, a *lower section* and an *upper section*, which refer to the vertical location of the thermocouples. Moreover, each riser

tube is connected to its own variac, whereas downcomer tubes are connected in pairs to two different variacs. Specifically, tube 5 and tube 6 form one pair, and tube 7 and tube 8 form the other one.

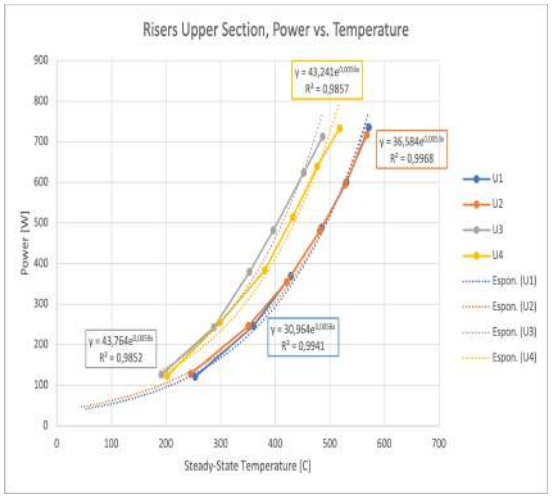

Figure 4.3: Heat Loss Test Riser Upper Level

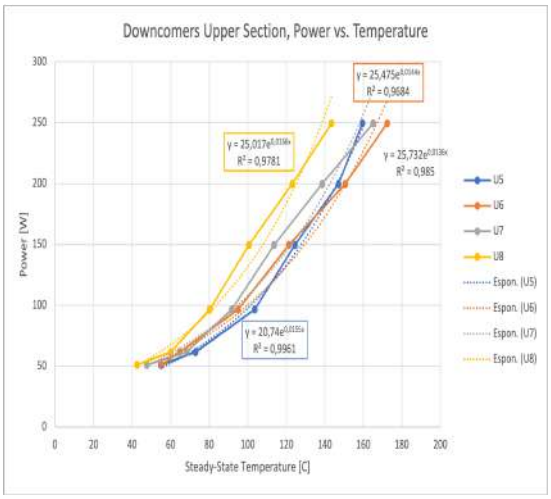

Figure 4.4: Heat Loss Test Downcomer Upper Level

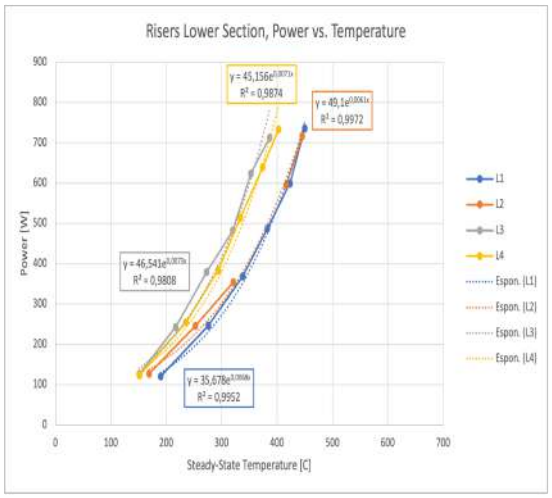

Figure 4.5: Heat Loss Test Riser Lower Level

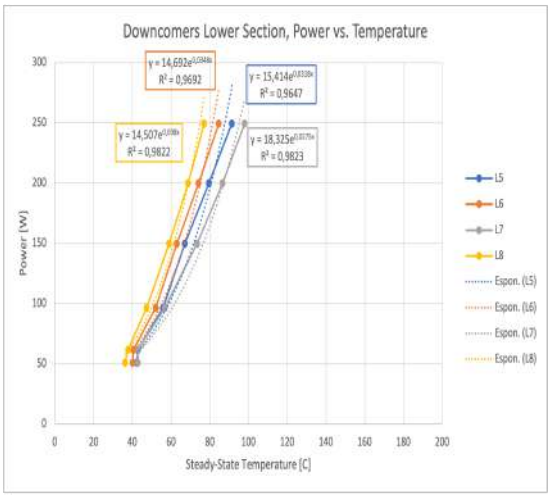

Figure 4.6: Heat Loss Test Downcomer Lower Level

In the previous graphs, the power lost to the environment is plotted as a function of the steady-state temperature. It is clear that each tube has its own characteristic behavior, and there are several reasons to explain it. Firstly, it is difficult to ensure that each variac provides the same power, since the delivery is controlled by a knob with which one can only select a percentage of the maximum available power. Moreover, the spot-welded

thermocouples introduce a certain degree of error in the measurement of the steady-state temperature and for this reason one curve might be shifted towards either the left of the right hand side of the graph. Additionally, each heater has its own resistance, meaning that the thermal power supplied to a tube is slightly different to the one supplied to the others. Lastly, it is important to remember that the thermal insulation was manually wrapped around the riser and downcomer tubes, meaning that it is reasonable to expect slightly different insulation efficiencies among different tubes.

For each data set, an exponential regression curve was calculated, in order to obtain a mathematical relationship between heat loss and steady-state temperature.

As it can be seen from the graphs, riser tubes 1 and 2 have the exact same behavior, as the two curves overlap each other. Instead, riser tubes 3 and 4, which in turn have a similar behavior, are affected by greater heat losses. This trend applies in both upper and lower section. With regards to downcomers, tube 8 has the greatest heat losses, especially in the upper section, while the other three downcomer tubes have a closer behavior.

Numerous attempts have been made with the goal of having a common behavior for all tubes, particularly by modifying the thermal insulation placing, but we decided to move forward in order to spend more time on the natural circulation experiments.

4.4 Natural Circulation Experiments

In this preliminary stage of the project, only nitrogen gas was used for the experiments, due to the high cost and limited availability of helium, that was used only in the pressure leak test in order to emphasize the different behavior with respect to nitrogen. In the future, experiments will be conducted in the natural circulation loop with helium gas and a mixture of nitrogen and helium gases as well.

In the following table, the most interesting investigated experimental conditions are reported. It is important to underline that other measurements have been carried out, but the following are more useful because they allow to make important comparisons.

Table 4.1: Investigated experimental conditions

Pressure *psi*	Riser Power *W*	Downcomer Power *W*
750	750	0
	685	
	625	
	560	
	500	
625	750	0
	685	
	625	
	560	
	500	

4.4.1 Experimental Procedure

Before running an experiment, the system undergoes a vacuum process using the building vacuum line available in the laboratory. Even though nitrogen is inert, meaning that a mixture with other gases is not hazardous, it is crucial to ensure that its physical properties are not affected by other species. Thus, the vacuum line is connected to the lower plenum for approximately 30 min before each run, in order to assure that also stagnant gases in the upper plenum are removed.

The experimental setup is then connected to the nitrogen tank and gas is injected in the

lower plenum till reaching the desired value of initial pressure. This operation is monitored using a pressure transducer in order to be as close as possible to the set value. At this time, approximately 10 min are given to the gas to uniformly distribute within the setup.

After these preliminary operations, heaters are switched on and set to the desire value of power, by controlling the percentage of output voltage supplied by the variacs. Between 10 and 20 min are then given before switching on the pulse generator, in order to establish a temperature difference between upper and lower plenum and allow nitrogen to move between upper and lower section by *natural circulation*. In fact, the heating Nichrome wire would be damaged in case of very low flow rate or even no flow. Each experiment took at least 8 h to reach a complete steady-state for riser inlet and outlet temperatures, while as it will be shown in the following steady-state conditions were not reached in both plena.

All variables measured in the system, such as temperature, pressure, power supplied to heating coils, are shown, monitored and saved using the program LabVIEW, acronym for *Laboratory Virtual Instrumentation Engineering Workbench*, which is an integrated development environment produced by National Instruments, an American company that develops automated test equipment and virtual instrumentation software. LabVIEW's most interesting characteristic is that it allows the user to visually develop complex measurement and control systems, without requiring the definition of any function or algorithm.

For the natural circulation experiments, all instruments installed in the system were connected to two different computers, after being grouped in 8 different DAQ modules. In this way, all variables of interest were shown, controlled and saved at the same time.

4.4.2 Heat Transfer Modeling

In this section, the heat transfer modeling is presented and discussed, including the simplifying assumptions that were made in order to accurately represent the heat transfer process.

The main goal of this analysis is to calculate the volumetric flow rate of nitrogen gas, that in turn allows the calculation of its velocity, which is to be compared with the thermal time-of-flight measurement for each tube. The starting point of the analysis is then reported in the following equation:

$$\dot{Q}_{\text{supplied}} = \dot{Q}_{\text{loss}} + \dot{Q}_{\text{gas}} \tag{4.1}$$

where $\dot{Q}_{\text{supplied}}$ represents the heat supplied to the gas through the heating coils, $\dot{Q}_{\text{loss}}$ represents the heat lost to the environment and $\dot{Q}_{\text{gas}}$ is the heat removed from the gas. The heat supplied through the heating coils is known, as well as the heat lost to the environment, because the regression curves in Figure 4.3 - 4.7 allow this calculation. The only unknown term is represented by the heat removed by the gas, which can be calculated as follows:

$$\dot{Q}_{\text{gas}} = \dot{m} \cdot c_p \cdot \Delta T \tag{4.2}$$

By reversing the above equation (4.2), it is possible to determine the mass flow rate as follows:

$$\dot{m} = \frac{\dot{Q}_{\text{gas}}}{c_p \cdot \Delta T} \tag{4.3}$$

It is necessary to remember that the mass flow rate equals the volumetric flow rate times the gas density, and the volumetric flow rate is given by the product between velocity and section. Thus, it is possible to determine the mathematical expression for the gas velocity within a single tube. It is given by the following equation:

$$v = \frac{4 \cdot \dot{m}}{\rho \cdot \pi \cdot D^2} \tag{4.4}$$

where ρ is the gas density and D the tube diameter.

The calculation of the gas density is complicated. In fact, all the fundamental assumptions underlying the ideal gas law are no longer valid, since at high pressure intermolecular forces and molecular volume cannot be neglected. Thus, the *van der Waals* equation is used for modeling the real gas behavior, far from the assumptions of ideal gas. The *van der Waals*

equation is the following:

$$(P + a \cdot \frac{n^2}{V^2}) \cdot (V - n \cdot b) = n \cdot R \cdot T \tag{4.5}$$

where a and b are positive constants, specific to a particular species. In the equation, the term $\frac{a}{V^2}$ takes into account the attractive forces between molecules, which make the effect of pressure less important than that predicted by the ideal gas law, and b for their finite volume.

Having to know the mass of nitrogen fed into the system, which is not possible, its density is estimated by first applying the ideal gas law and then verified using online software that return an estimate of the gas density by knowing temperature and pressure conditions. By referring to (4.3), gas velocity depends on the amount of heat removed from the gas, which in turn depends on the heat supplied by the heating coil and the one lost to the environment.

The determination of the heat lost is also not direct. In fact, while it is true that there are empirical relationships for determining heat losses, these were calculated for two wall temperature measurement points only. As a result, the regression curves are theoretically valid only for these two measurement spots. Thus, for calculating the heat lost, an important simplifying assumption was made: the heat losses are assumed to be the sum of two separate contributions, that is, half due to the lower half of the tube, described by the regression curve calculated in the lowest measurement point, and half due to the upper half, described by the regression curve calculated in the highest measurement point. Moreover, the temperature is assumed to be constant and equal to the mean value.

In the gas velocity measurement, only the four riser tubes are considered for heat losses, because the thermal time-of-flight sensors are installed in the riser tubes only. The eight

regression curves are reported below. The set of regression equations is reported below.

$$\begin{cases} Q_{loss,1U} = 30.964e^{0.0056 \cdot T} \\ Q_{loss,2U} = 36.584e^{0.0053 \cdot T} \\ Q_{loss,3U} = 43.764e^{0.0059 \cdot T} \\ Q_{loss,4U} = 43.241e^{0.0056 \cdot T} \\ Q_{loss,1L} = 35.678e^{0.0068 \cdot T} \\ Q_{loss,2L} = 49.1e^{0.0061 \cdot T} \\ Q_{loss,3L} = 46.541e^{0.0073 \cdot T} \\ Q_{loss,4L} = 45.156e^{0.0071 \cdot T} \end{cases}$$

The heat loss for the i-th tube are given by the following equation:

$$\dot{Q}_{i,TOT} = \frac{1}{2}\dot{Q}_{i,U} + \frac{1}{2}\dot{Q}_{i,L} \tag{4.6}$$

By plugging the correct temperature value in each regression curve, it is possible to determine the heat lost to the environment.

Table 4.2: Heat loss data for different experimental conditions

Experiment	$\dot{Q}_{1,LOSS}$ W	$\dot{Q}_{2,LOSS}$ W	$\dot{Q}_{3,LOSS}$ W	$\dot{Q}_{4,LOSS}$ W
3V_0V_750 psi	327	328	383	392
2.75V_0V_750 psi	304	304	409	355
2.5V_0V_750 psi	264	272	337	321
2.25V_0V_750 psi	230	238	273	274
2V_0V_750 psi	207	215	241	246
3V_0V_625 psi	348	345	399	420
2.5V_0V_625 psi	279	283	305	332
2.25V_0V_625 psi	240	244	267	284
2V_0V_625 psi	227	232	252	276

4.5 Natural Circulation Results

4.5.1 Pressure and Temperature Profiles

The most interesting and valuable results from the natural circulation loop are presented and discussed in this section. In order to better understand the following graphs, Fig. 2.3 is shown here.

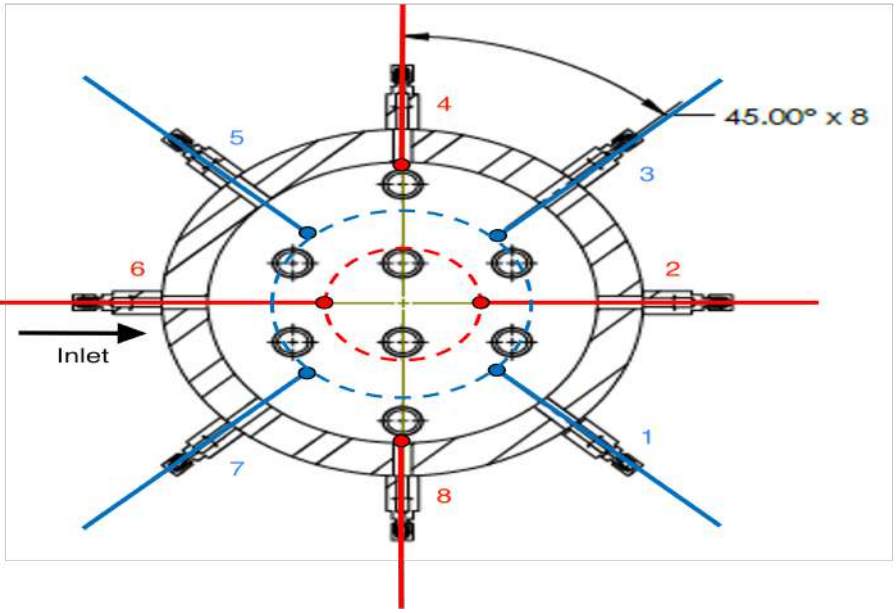

Figure 4.7: Thermocouple placing

As already described in the previous chapter, it is logical to identify different sets of thermocouples. In particular, in each plenum there is an upper level and a lower level, referring to the different vertical location of the radial thermocouples. Similarly, two levels can also be identified for wall thermocouples, which will be referred to as *wall thermocouple lower level* (WL) and *wall thermocouple upper level* (WU). Lastly, RI and RO refer to the set of thermocouples measuring tube inlet temperatures and tube outlet temperatures, respectively. All the graphs shown in the following are taken from a specific experiment, in particular the one in which 3 V were supplied to the heating coil on the riser tubes and no power was supplied to downcomer tubes, in order to maximize the natural circulation, starting with an initial nitrogen pressure of approximately 750 psi.

First of all, it is important to show the temporal evolution of the pressure and temperature profiles within the system.

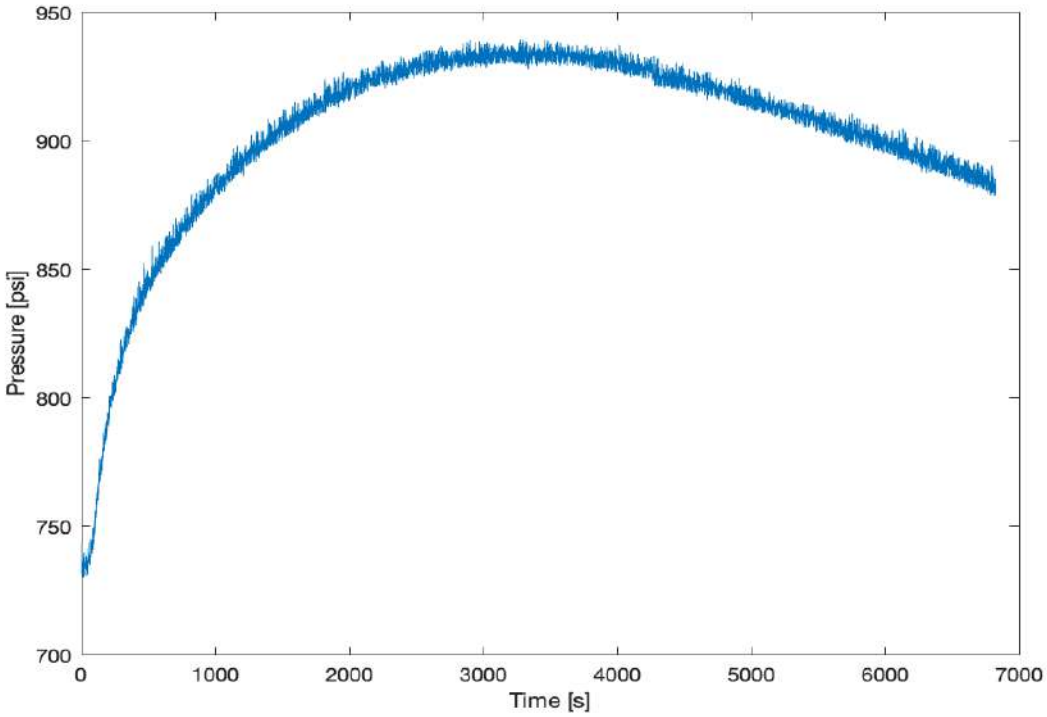

Figure 4.8: Pressure profile

In Figure 4.8 the pressure profile is shown. The first increase in pressure is due to the increment in nitrogen temperature, which makes the pressure reach almost 950 psi. However, when the temperature stabilizes, pressure does not increase any further, and in fact it decreases due to the presence of leaks, as already discussed in the pressure leak test paragraph. It has to be mentioned that the pressure does not change significantly over time, as the leak rate is slightly below 30 psi h^{-1}, or equivalently slightly below 2 bar h^{-1}.

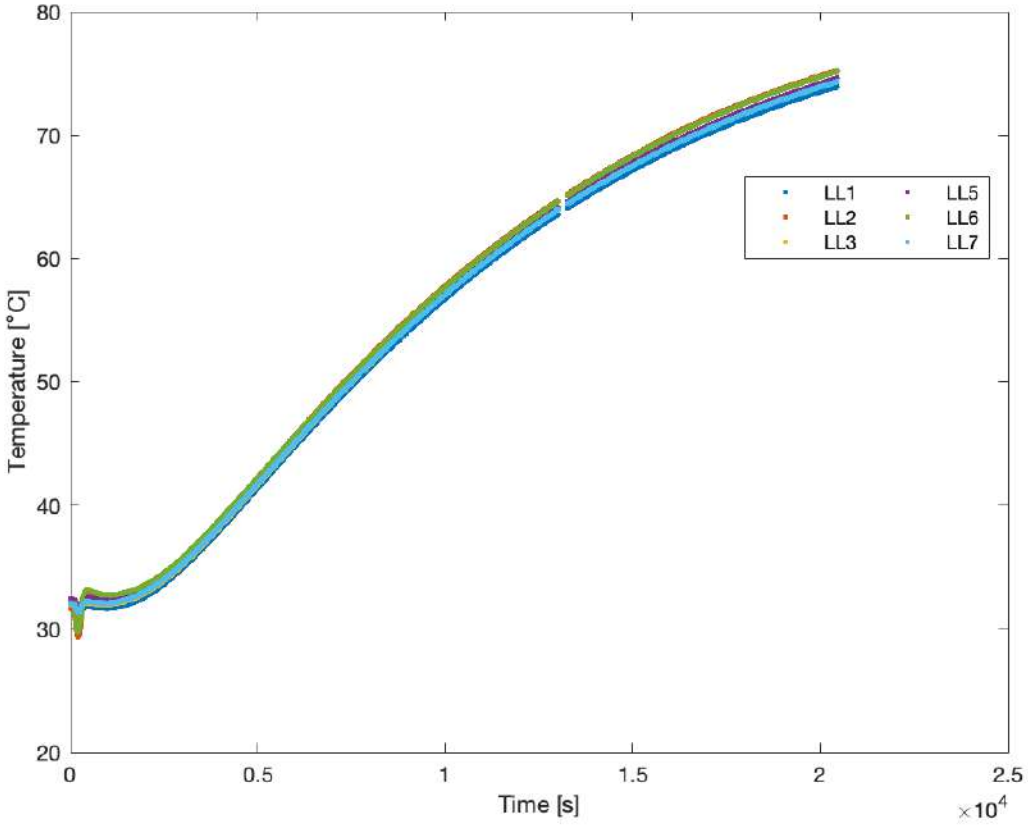

Figure 4.9: Lower Plenum Lower Level temperature profiles

In Figure 4.9, the temporal evolution of the temperatures within the lower plenum in the lower level is shown. As it can be seen from the image, a fully complete steady state is not reached. Experiments have highlighted that it is not possible to reach steady state in the lower section of the lower plenum within a reasonable time frame. In fact, each experiment was executed for several consecutive hours, already overloading in several cases the data analysis system. It has also to be mentioned that the temperature profile in the lower section of the lower plenum is not of paramount importance for the experiment, thus not reaching a fully complete steady state does not represent a limitation to the experimental data set. The curves practically overlap, which means that the gas is well mixed and no hot-spots are expected in this section.

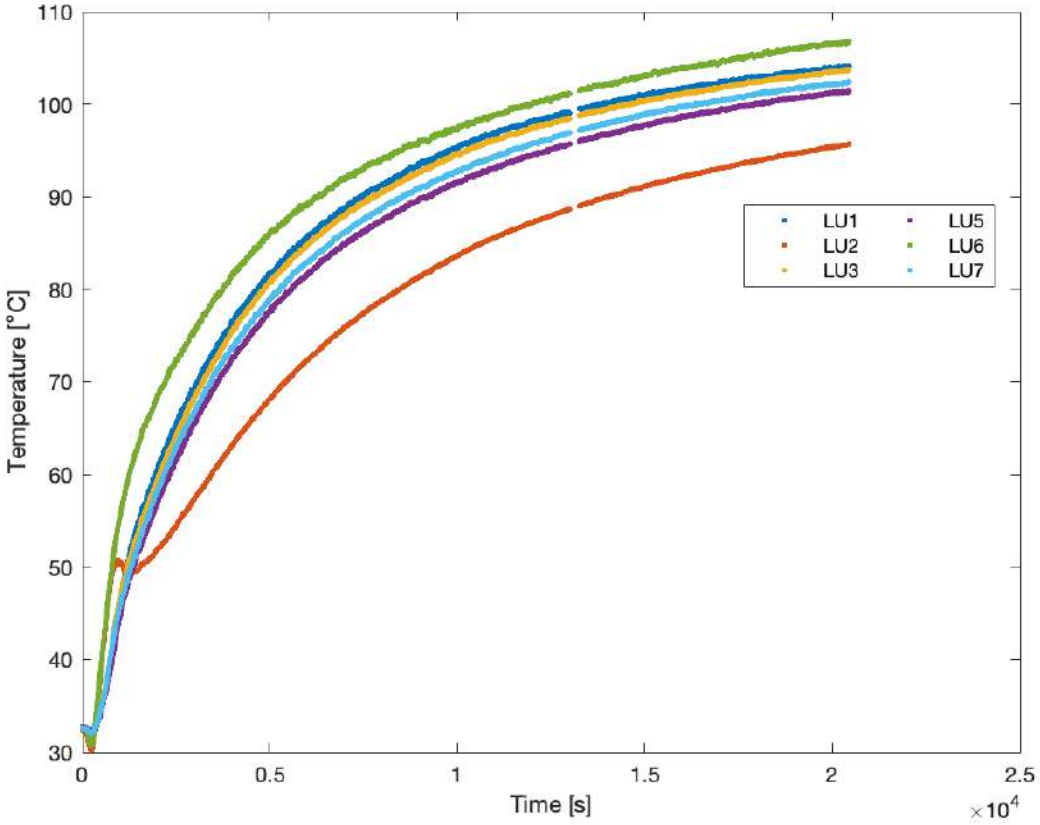

Figure 4.10: Lower Plenum Upper Level temperature profiles

In Figure 4.10, the temporal evolution of the temperatures within the lower plenum in the upper level is shown. What was said above for the lower plenum lower level also applies here, concerning the non steady state profile of temperature. In addition, all the curves are very close together, with the only exception of the curve for the thermocouple in position 2. Referring to Fig. 4.7, thermocouples at position 2 and 6 measure the temperature at points very close together, and there is no obvious reason why the two temperature values are so far apart. For this reason, it can be assumed that the thermocouple measuring the temperature in position 2 has some kind of calibration problems.

Moreover, it is important to mention that a few standard deviations have been calculated by varying a window width over which the function was calculated in both cases, and it is always well below the unit value, meaning that in each specific window each temperature value is very close to the average value calculated in the window.

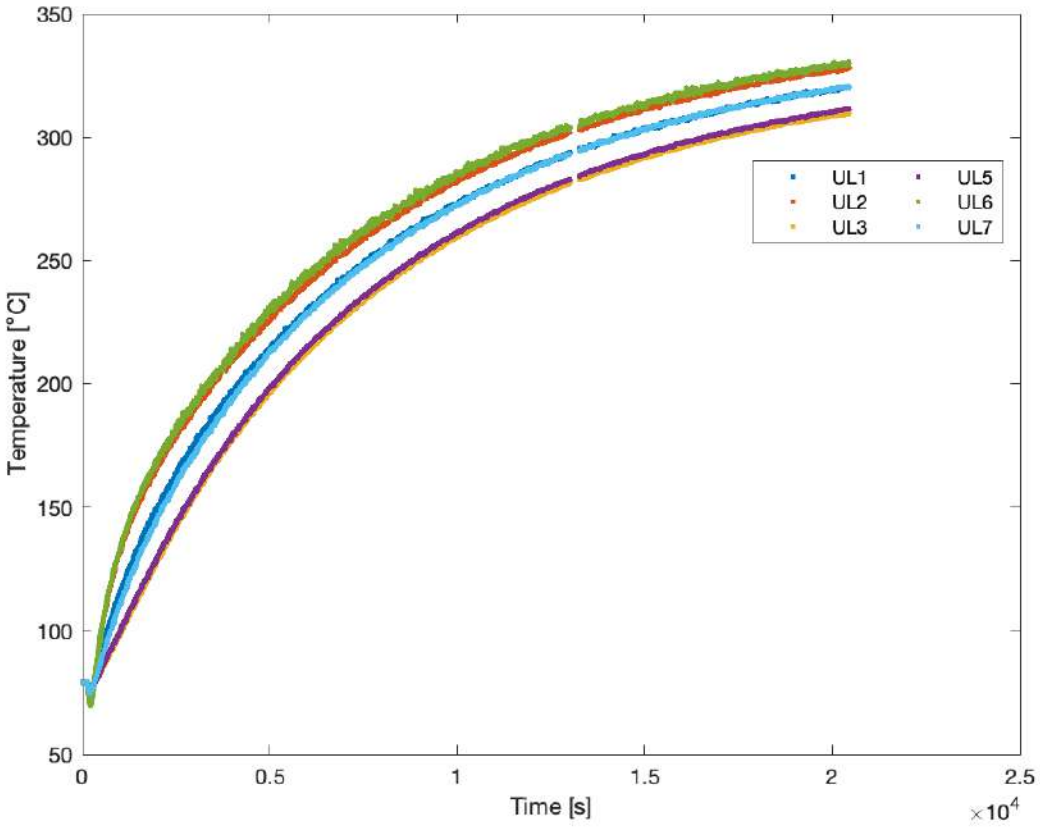

Figure 4.11: Upper Plenum Lower Level temperature profiles

In Figure 4.11, the temporal evolution of the temperatures within the upper plenum in the lower level is shown. The most interesting result to highlight here is that UL2 is very similar to UL6 and these are the highest temperature values measured in all experiments. This is followed by the values measured in UL1 and UL7, which in turn are higher than those in UL5 and UL3. These trends are also confirmed by the temperatures measured at tubes' outlets, as downcomer tubes 6 and 8, close to UL7 and UL1, respectively, have a higher temperature than downcomer tubes 5 and 7, close to UL5 and UL3, respectively.

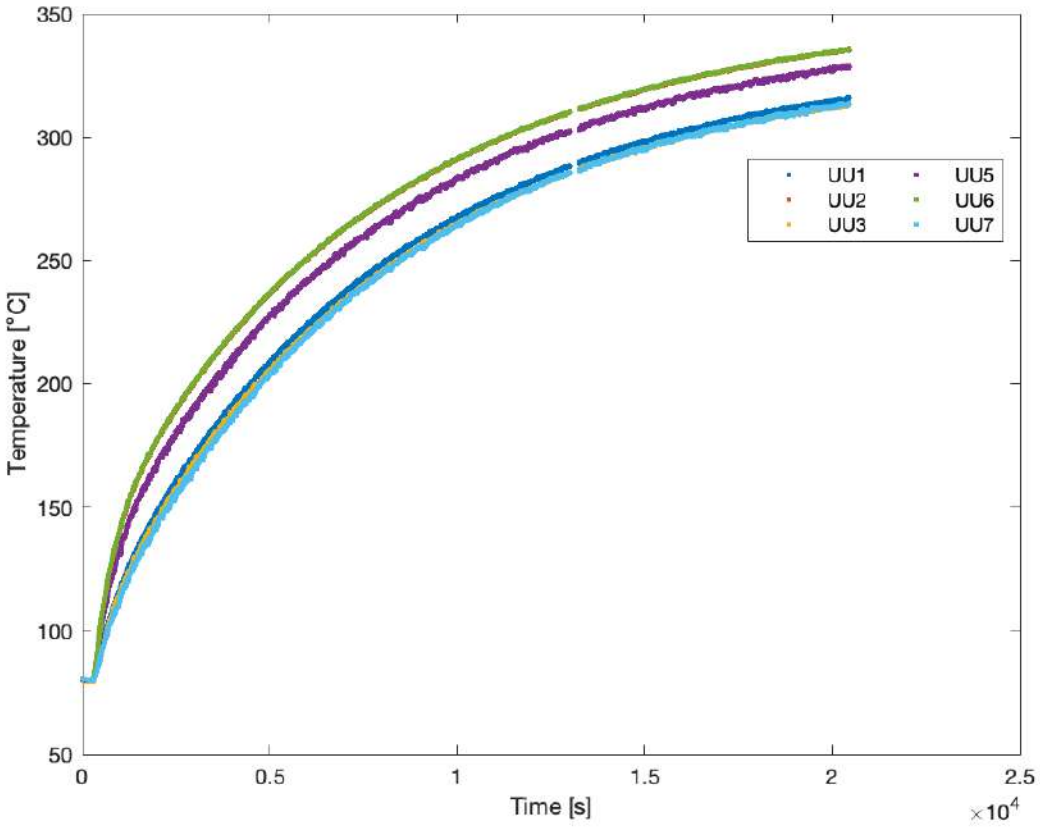

Figure 4.12: Upper Plenum Upper Level temperature profiles

In Figure 4.12, the temporal evolution of the temperatures within the upper plenum in the upper level is shown. The most interesting result to highlight here is that UU2 and UU6, for all the conducted experiments, have always the same value, with a maximum difference of $\pm 1°C$, significantly greater than that measured by the other thermocouples. This is due to the fact that the above mentioned measurement points are located above the outlet of riser tubes 2 and 3, from which the gas rises by natural circulation.

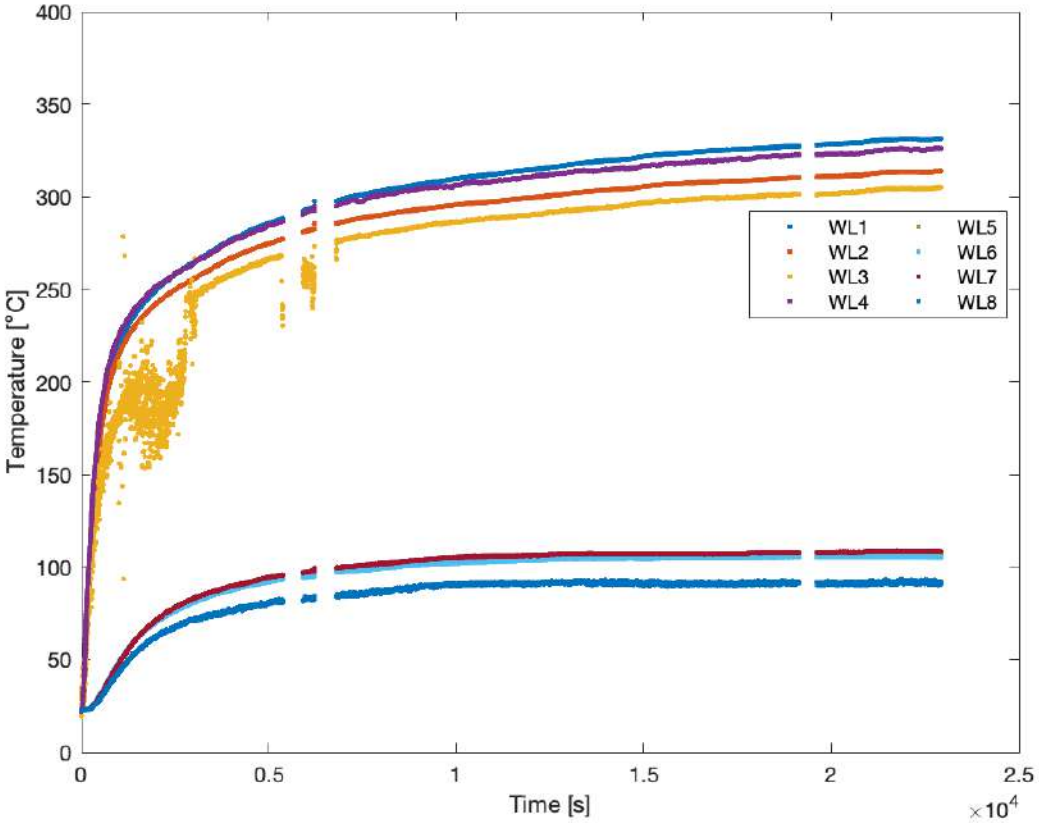

Figure 4.13: Wall Lower Level temperature profiles

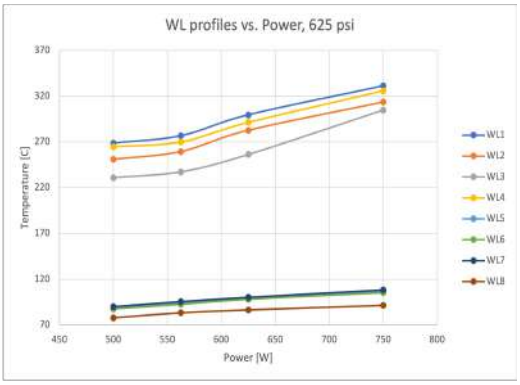

Figure 4.14: WL profiles vs. Power, 625 psi

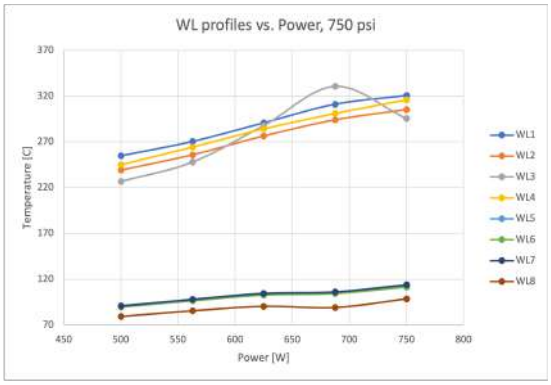

Figure 4.15: WL profiles vs. Power, 750 psi

In Figure 4.13, the temporal evolution of the wall temperatures in the lower level is shown. As it can be seen from the image, in this case steady state can be considered to have been reached, as the temperature does not change by more than 2 $^{\circ}\mathrm{C\,h^{-1}}$. In addition, the spot-welded thermocouple on riser tube number 3 has always been problematic, and this

explains the sluggish behavior in the first part of the graph.

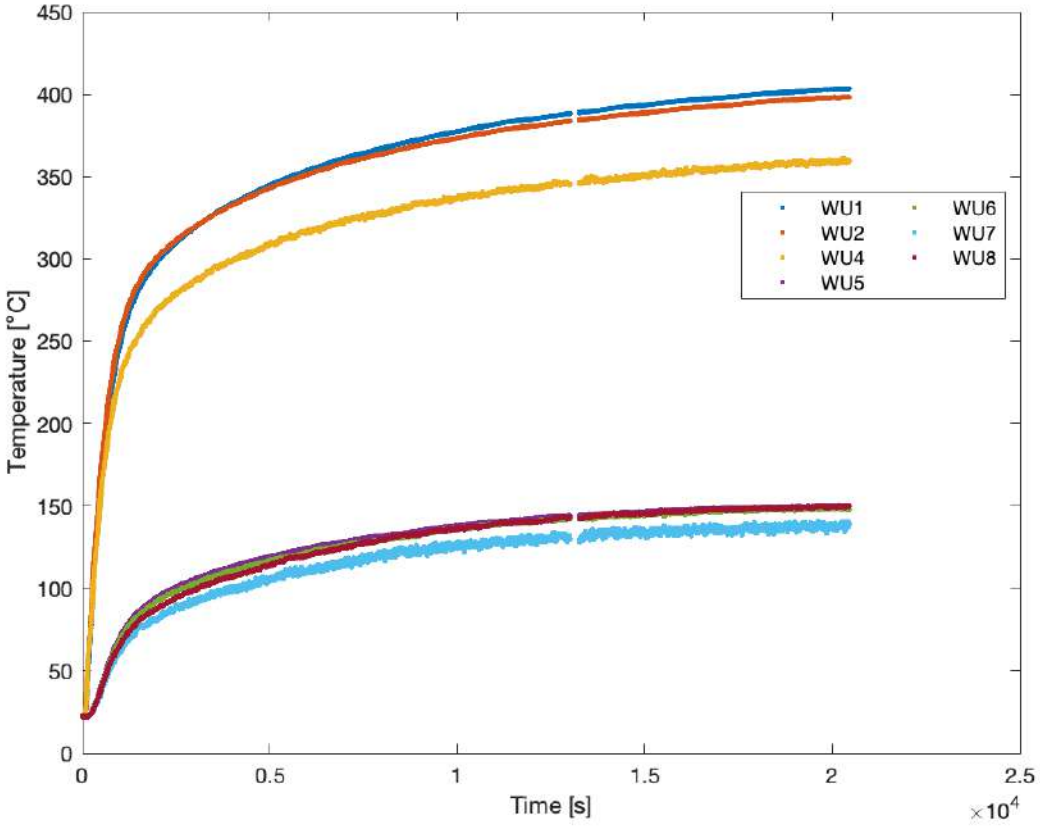

Figure 4.16: Wall Upper Level temperature profiles

Figure 4.17: WU profiles vs. Power, 625 psi

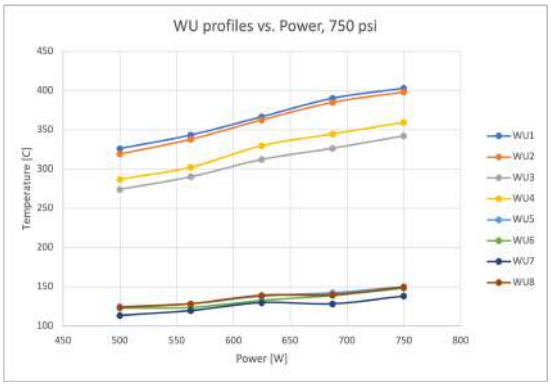

Figure 4.18: WU profiles vs. Power, 750 psi

In Figure 4.16, the temporal evolution of the wall temperatures in the upper level is shown. What has been said about the steady state for the previous graph also applies here. In contrast, in Figure 4.13 the riser tube number 3 temperature profile is not shown,

as the signal resulted to be extremely noisy and sluggish.

In both cases, the predicted trend already discussed in the heat loss section is confirmed: riser tubes 1 and 2 have very similar behavior, with smaller heat losses allowing them to reach a higher temperature, while riser tubes 3 and 4, with larger heat losses, reach temperatures that can be as much as 60 °C lower than those of the other two tubes.

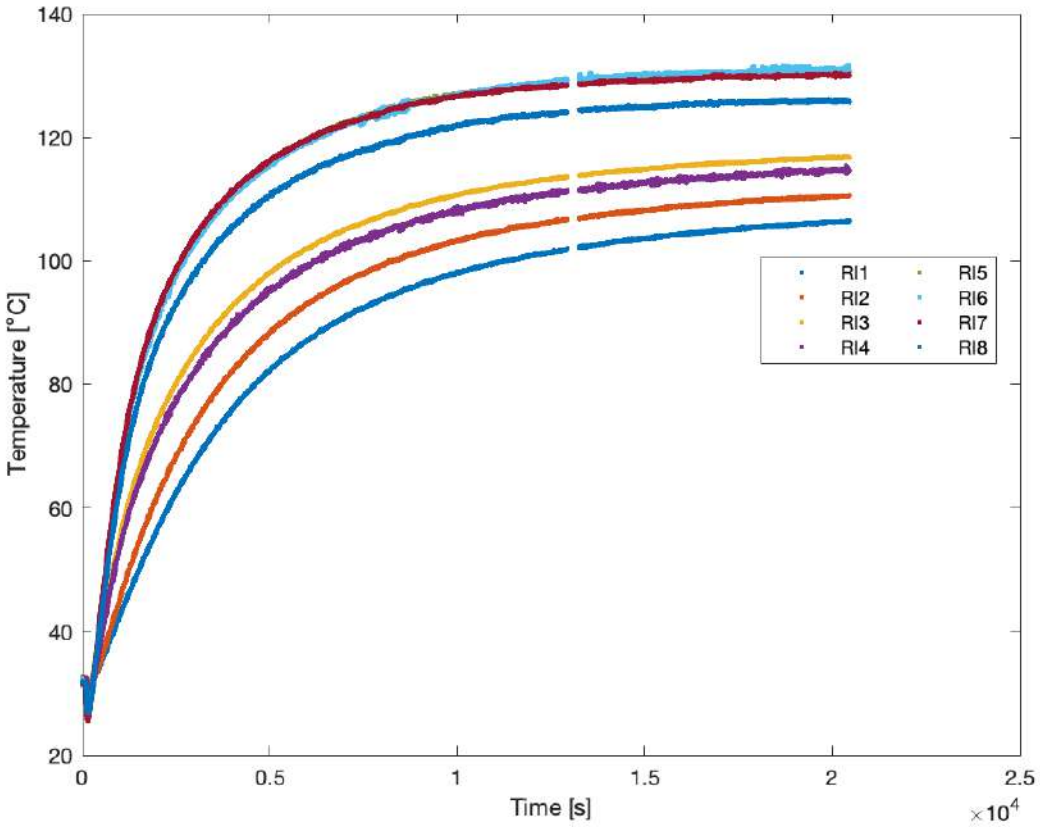

Figure 4.19: Tube Inlet temperature profiles

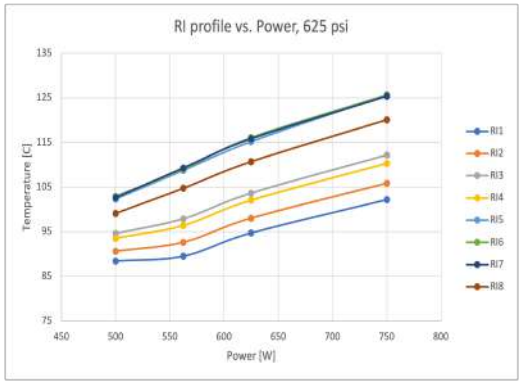

Figure 4.20: RI profiles vs. Power, 625 psi

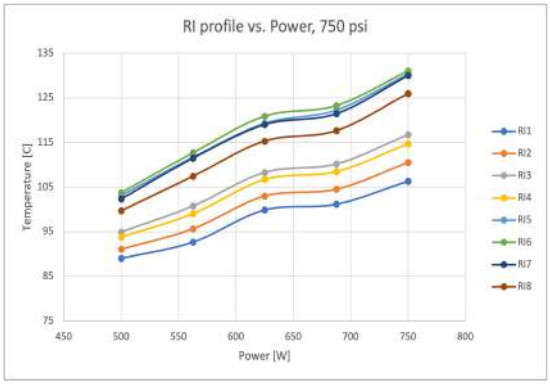

Figure 4.21: RI profiles vs. Power, 750 psi

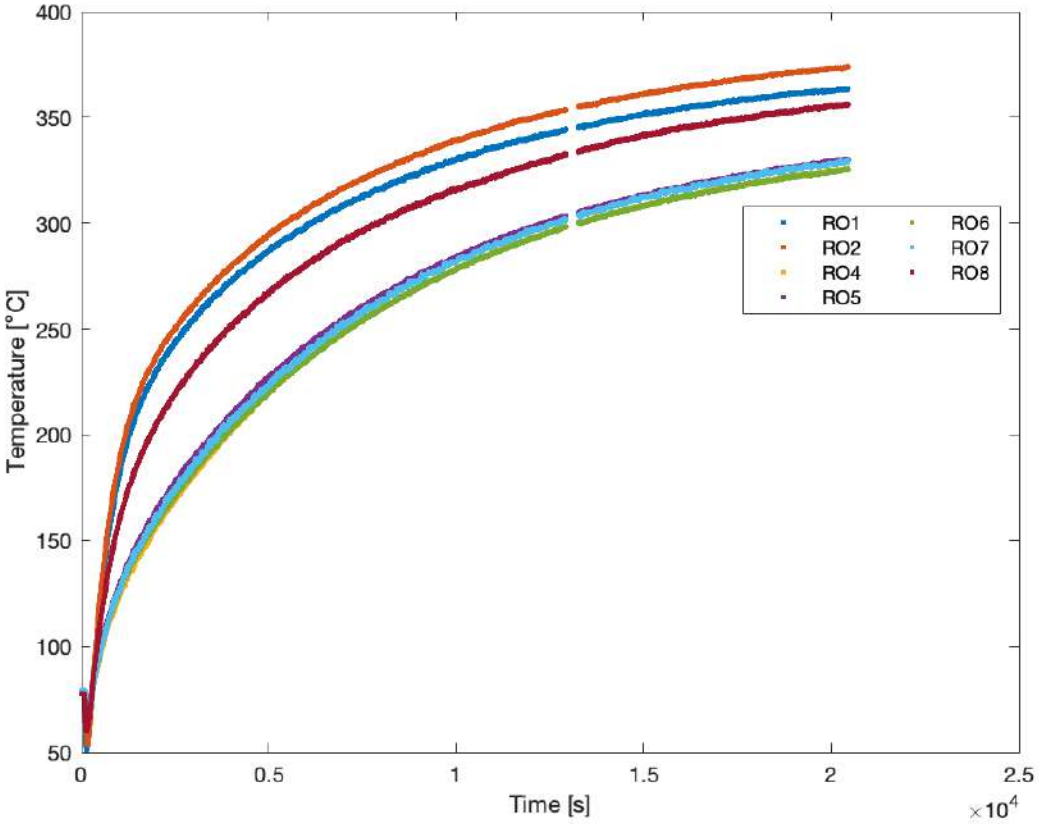

Figure 4.22: Tube Outlet temperature profiles

Figure 4.23: RO profiles vs. Power, 625 psi

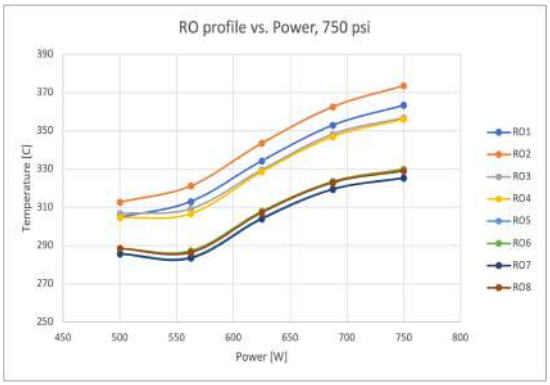

Figure 4.24: RO profiles vs. Power, 750 psi

In Figure 4.19 and Figure 4.22, the temporal evolution of the tubes' inlet and outlet temperatures in the lower and upper plenum is shown, respectively.

The most interesting result to be shown here is that the temperature measured at the inlet of the downcomer tubes is greater that that at the inlet of riser tubes, while the outlet

temperature of the riser tubes is significantly higher than that at the outlet of downcomer tubes. This fact confirms the presence of natural circulation, emphasizing that the gas rises in the inner section of the system and, after mixing in the upper plenum, descends through the downcomer tubes.

It is important to know that each experiment has different temperature and pressure values, but the trends shown in the previous figures are common to all of them.

The last significant graph that needs to be reported is the one showing the trend of temperature difference between inlet and outlet of riser tubes as a function of the power supplied to the heating coils, for two different values of nitrogen initial pressure.

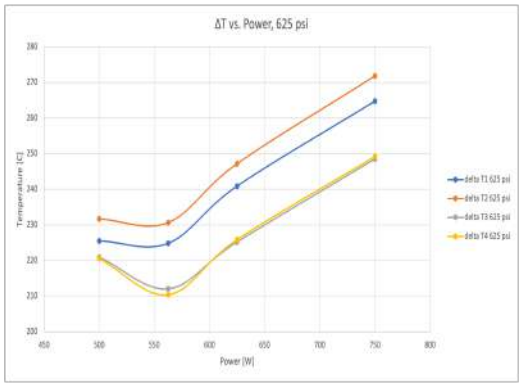

Figure 4.25: $\Delta(T)$ as a function of power for riser tubes, 625 psi

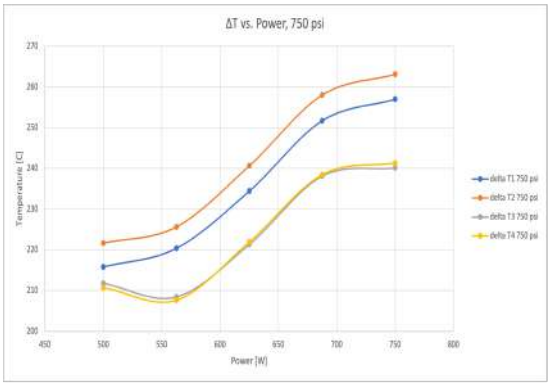

Figure 4.26: $\Delta(T)$ as a function of power for riser tubes, 750 psi

The obvious result to emerge from these two graphs is that the gas in riser tubes 1 and 2 has a significantly greater temperature rise than that in riser tubes 3 and 4, which, on the other hand, have very similar behavior between them. This is in complete agreement with the results obtained from the heat loss tests discussed earlier in the chapter: in steady state conditions, greater heat losses imply less heat removed by the gas, and consequently also less of its temperature rise.

4.5.2 Thermal Time of Flight Sensor Results

As already stated in the Instrumentation Chapter, each riser tube has its own thermal time of flight sensor, which is unique and different from all others. This is because each

sensor was built and assembled by hand, and as a result it is reasonable to assume that the sensing element of each thermocouple will not be perfectly at the center line. Considering a laminar flow, which takes place in the natural circulation loop since the Reynolds number is well below 2000, the well-known parabolic velocity profile is expected, meaning that the measured velocity depends on the radial location of the thermocouple sensing element.

In the following section, time of flight sensor results will be reported and discussed only for riser tubes 1, 3 and 4, as on riser tube 2 an optical fiber sensor, developed by *The University of Pittsburgh*, was installed. The thermocouple sampling rate in the time of flight sensors was set to 100 Hz, meaning that 100 temperature measurement were taken in the time interval of 1 s. A high sampling rate is needed for the time of flight sensor, since the gas velocity measurement depends precisely on the accuracy with which the heat pulse passage can be detected. However, a negative consequence of the high sampling frequency is the processing of a large amount of data, which therefore does not allow monitoring the velocity profile at all stages of the experiment, but only when steady-state is reached.

In the following, graphs for riser tubes 1, 3 and 4 will be presented and discussed, showing the trends of the expected velocity, obtained from the energy balance, and of the measured velocity from the time of flight sensors, as a function of the power input to the riser tubes' heating coils, for two different values of the initial nitrogen pressure.

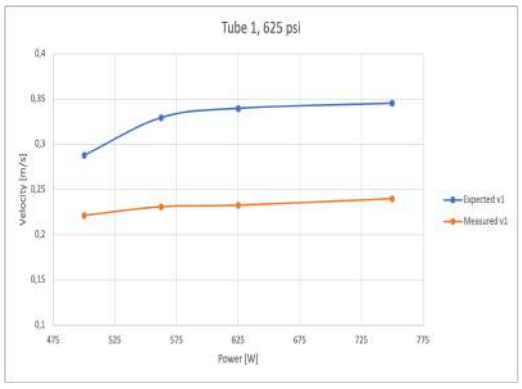

Figure 4.27: Tube 1 profiles with initial nitrogen pressure of 625 psi

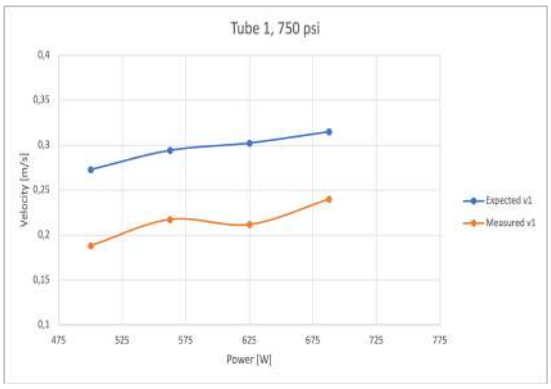

Figure 4.28: Tube 1 profiles with initial nitrogen pressure of 750 psi

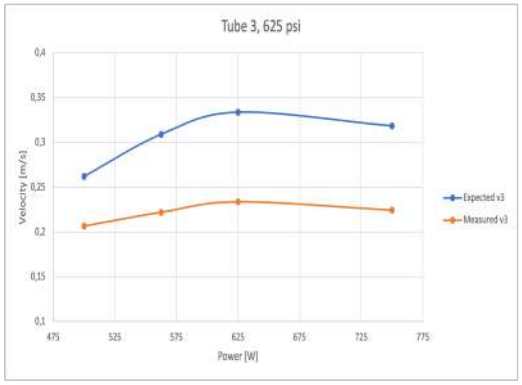

Figure 4.29: Tube 3 profiles with initial nitrogen pressure of 625 psi

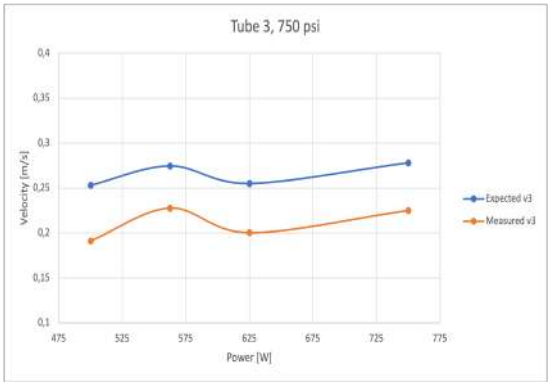

Figure 4.30: Tube 3 profiles with initial nitrogen pressure of 750 psi

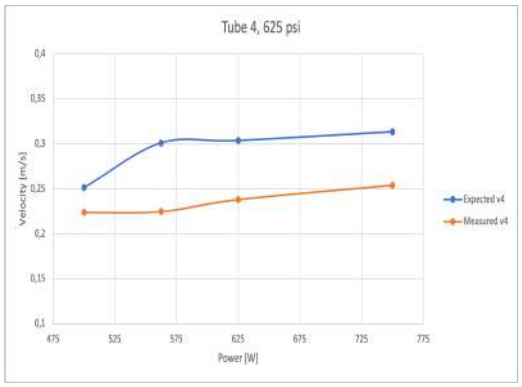

Figure 4.31: Tube 4 profiles with initial nitrogen pressure of 625 psi

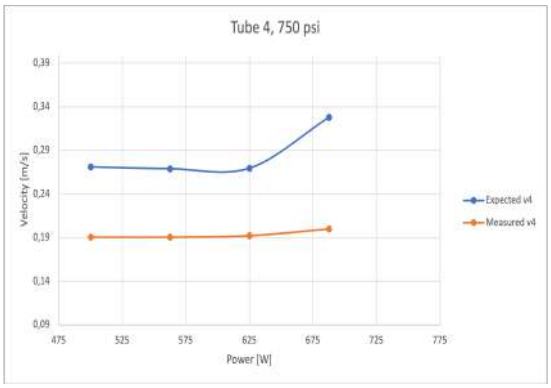

Figure 4.32: Tube 4 profiles with initial nitrogen pressure of 750 psi

In all the graphs, it can be seen that the expected velocity, calculated from the energy balance, is higher than the one measured with the time of flight sensors. The reason for this trend is not certain and yet has to be investigated further. However, it was supposed that the gas velocity profile was parabolic, characteristic of a laminar flow. This could be a forced assumption, as the gas travels a limited space between entering from the lower plenum in the riser tubes to the time of flight sensors. For this reason, it is possible to assume that the velocity profile is not fully developed and yet the parabolic shape does not apply. However, it is important to underline that energy balance and time of flight sensors give trends with the same shape.

Table 4.3: Relative errors between measured and expected velocities for different experimental conditions

Experiment	$v_{1,\text{err}}$	$v_{3,\text{err}}$	$v_{4,\text{err}}$
3V_0V_750 psi	-	0,13	0,38
2.75V_0V_750 psi	0,24	-	0,39
2.5V_0V_750 psi	0,30	0,21	0,29
2.25V_0V_750 psi	0,26	0,17	0,29
2V_0V_750 psi	0,31	0,24	0,30
3V_0V_625 psi	0,31	0,30	0,19
2.5V_0V_625 psi	0,32	0,30	0,22
2.25V_0V_625 psi	0,30	0,28	0,25
2V_0V_625 psi	0,23	0,21	0,11

As it can be seen from Table 4.3, the time of flight sensor installed in riser tube 1 gives a stable relative error between the expected and measured velocities, being around 30%. Moreover, riser tube 1 and 3 time of flight sensors show the same behavior for the experiments conduced with nitrogen initial pressure of 625 psi, with the one on riser tube 1 being slightly more accurate. Instead, it is more difficult to identify a regular trend for the relative error for the time of flight sensor installed on riser tube 4, since it significantly varies, especially under the experimental conditions mentioned above.

Chapter 5

Conclusions

During his time at *The City College of New York*, the Candidate firstly dealt with the construction of the experimental setup, assisted by a team of collaborators, dealing with different issues regarding the stability, positioning and configuration of the structure, but also technical inconvenience in the actual assembly of the reactor. Secondly, he installed measurement devices, such as thermocouples and pressure transducer, and developed a data collection and processing system. Finally, he personally conducted the natural circulation experiments and performed the analysis of collected data.

As reported by several authors [2], [4], [5], [11] and many others, natural circulation test facilities studied so far generally consist of a heat source, a heat sink and two connection pipes. However, the one channel flow configuration does not allow the investigation of upward/downward/stagnant flow distribution between multiple parallel flow passages. For this reason, the facility setup present at *The City College of New York* is unique and it simulates more precisely what happens inside a nuclear reactor core.

At this early stage of the project, natural circulation experiments were conducted using nitrogen only, while in the future they will be performed using a mixture of nitrogen and helium and pure helium as well. This will be done in order to simulate the flow loops with the actual gas that is used inside many nuclear reactors and thus obtain more significant

data.

From the results reported in the previous chapter, it can be seen that, although there is no perfect mixing in either plena, a stable regime of natural circulation is established between lower and upper plenum, with the gas distributing almost evenly in the riser tubes. The gas flow measurement is performed using a novel thermal time of flight sensor, which can work in the presence of high temperatures and pressures. Velocities measured by each sensor are always significantly lower than the expected one, calculated with the energy balance. This implies that changes will be made to the sensors in the future, and it is thought that mainly the position of the thermocouples' sensing elements may not be accurate. In addition, CFD models will help in understanding the actual velocity profile in the sensors region, which may also be not parabolic.

Bibliography

[1] Nisrene M. Ahmed, Puzhen Gao, and Solomon Bello. Natural circulation systems in nuclear reactors: Advantages and challenges. In *IOP Conference Series: Earth and Environmental Science*, volume 467. Institute of Physics Publishing, 4 2020.

[2] W. Ambrosini, N. Forgione, J. C. Ferreri, and M. Bucci. The effect of wall friction in single-phase natural circulation stability at the transition between laminar and turbulent flow. *Annals of Nuclear Energy*, 31:1833–1865, 11 2004.

[3] M Ashauer, H Glosch, F Hedrich, N Hey, H Sandmaier, and W Lang. Thermal flow sensor for liquids and gases based on combinations of two principles.

[4] Dipankar N. Basu, Souvik Bhattacharyya, and P. K. Das. Effect of heat loss to ambient on steady-state behaviour of a single-phase natural circulation loop. *Applied Thermal Engineering*, 27:1432–1444, 6 2007.

[5] Dipankar Narayan Basu, Souvik Bhattacharyya, and P. K. Das. Effect of geometric parameters on steady-state performance of single-phase ncl with heat loss to ambient. *International Journal of Thermal Sciences*, 47:1359–1373, 10 2008.

[6] Walter Borreani, Davide Chersola, Guglielmo Lomonaco, and Mario Misale. Assessment of a 2d cfd model for a single phase natural circulation loop. *International Journal of Heat and Technology*, 35:S300–S306, 9 2017.

[7] Chan Byon. Numerical and analytic study on the time-of-flight thermal flow sensor.

International Journal of Heat and Mass Transfer, 89:454–459, 6 2015.

[8] E. Engelien, O. Ecin, R. Viga, B. J. Hosticka, and A. Grabmaier. Calibration-free volume flow measurement principle based on thermal time-of-flight (ttof). In *Procedia Engineering*, volume 25, pages 765–768, 2011.

[9] Darius Lisowski, Qiuping Lv, Bogdan Alexandreanu, Yiren Chen, Rui Hu, and Tanju Sofu. Technical letter report: An overview of non-lwr vessel cooling systems for passive decay heat removal final report.

[10] Allison J. Mahvi, Bachir El Fil, and Srinivas Garimella. Accurate and inexpensive thermal time-of-flight sensor for measuring refrigerant flow in minichannels. *International Journal of Heat and Mass Transfer*, 132:184–193, 4 2019.

[11] Seyed Khalil Mousavian, Mario Misale, Francesco D'Auria, and Mahmoud A. Salehi. Transient and stability analysis in single-phase natural circulation. *Annals of Nuclear Energy*, 31:1177–1198, 7 2004.

[12] D. S. Pilkhwal, W. Ambrosini, N. Forgione, P. K. Vijayan, D. Saha, and J. C. Ferreri. Analysis of the unstable behaviour of a single-phase natural circulation loop with one-dimensional and computational fluid-dynamic models. *Annals of Nuclear Energy*, 34:339–355, 5 2007.

[13] Ibrahim A. Said, Mahmoud M. Taha, Shoaib Usman, and Muthanna H. Al-Dahhan. Effect of helium pressure on natural convection heat transfer in a prismatic dual-channel circulation loop. *International Journal of Thermal Sciences*, 124:162–173, 2 2018.

[14] Ibrahim A. Said, Mahmoud M. Taha, Shoaib Usman, Brian G. Woods, and Muthanna H. Al-Dahhan. Investigation of natural convection heat transfer in a unique scaled-down dual-channel facility. *AIChE Journal*, 63:387–396, 1 2017.